Technical Report Documentation Page

1. Report No. FHWA/TX-16/0-6878-1	2. Government Accession No.	3. Recipient's Catalog No.
4. Title and Subtitle International Center for Partnered Pavement Preservation (ICP3): First Year Progress Report		5. Report Date August 2015; Published June 2016 6. Performing Organization Code
7. Author(s) Jorge A Prozzi, Andre Smit, Pedro Serigos, Sareh Kouchaki		8. Performing Organization Report No. 0-6878-1
9. Performing Organization Name and Address Center for Transportation Research The University of Texas at Austin 1616 Guadalupe Street, Suite 4.202 Austin, TX 78701		10. Work Unit No. (TRAIS) 11. Contract or Grant No. 0-6878
12. Sponsoring Agency Name and Address Texas Department of Transportation Research and Technology Implementation Office P.O. Box 5080 Austin, TX 78763-5080		13. Type of Report and Period Covered Technical Report April 2015–August 2015 14. Sponsoring Agency Code
15. Supplementary Notes Project performed in cooperation with the Texas Department of Transportation and the Federal Highway Administration.		

16. Abstract

The Accelerating Innovation in Partnered Pavement Preservation project was initiated to promote and streamline research in the area of pavement preservation and to optimize the use of TxDOT's research and implementation resources by fostering cooperation and collaboration with the US DOT Center for Highway Pavement Preservation (CHPP). CHPP is a research and innovation partnership lead by Michigan State University which members include: The University of Texas at Austin, The University of Illinois at Urbana-Champaign, The University of Minnesota, The University of Hawaii at Manoa and North Carolina A&T University.

This preliminary progress report summarizes the work performed during the first five months of the project, from April to August 2015. During this period two task orders were developed and the corresponding work was planned and initiated. This report also presents the initial findings of these two task orders. The two task orders are: 1) Determination of Field Performance of Thin Overlays Relative to Alternative Preservation Techniques and 2) Quantification of Highway Pavement Surface Micro- and Macro-Texture.

17. Key Words Pavement Preservation, Preventive Maintenance, Surface Treatments, Thin Overlays, Surface Texture, Skid Resistance, Friction.	18. Distribution Statement No restrictions. This document is available to the public through the National Technical Information Service, Springfield, Virginia 22161; www.ntis.gov.

19. Security Classif. (of report) Unclassified	20. Security Classif. (of this page) Unclassified	21. No. of pages 60	22. Price

Form DOT F 1700.7 (8-72) Reproduction of completed page authorized

THE UNIVERSITY OF TEXAS AT AUSTIN
CENTER FOR TRANSPORTATION RESEARCH

International Center for Partnered Pavement Preservation (ICP3): First Year Progress Report

Jorge A Prozzi
Andre Smit
Pedro Serigos
Sareh Kouchaki

CTR Technical Report:	0-6878-1
Report Date:	August 2015; Published June 2016
Project:	0-6878
Project Title:	Accelerating Innovation in Partnered Pavement Preservation
Sponsoring Agency:	Texas Department of Transportation
Performing Agency:	Center for Transportation Research at The University of Texas at Austin

Project performed in cooperation with the Texas Department of Transportation and the Federal Highway Administration.

Center for Transportation Research
The University of Texas at Austin
1616 Guadalupe, Suite 4.202
Austin, TX 78701

http://ctr.utexas.edu/

Disclaimers

Author's Disclaimer: The contents of this report reflect the views of the authors, who are responsible for the facts and the accuracy of the data presented herein. The contents do not necessarily reflect the official view or policies of the Federal Highway Administration or the Texas Department of Transportation (TxDOT). This report does not constitute a standard, specification, or regulation.

Patent Disclaimer: There was no invention or discovery conceived or first actually reduced to practice in the course of or under this contract, including any art, method, process, machine manufacture, design or composition of matter, or any new useful improvement thereof, or any variety of plant, which is or may be patentable under the patent laws of the United States of America or any foreign country.

Engineering Disclaimer

NOT INTENDED FOR CONSTRUCTION, BIDDING, OR PERMIT PURPOSES.

Research Supervisor: Jorge Prozzi

Acknowledgments

The authors express appreciation to Mr. Wade Odell who was instrumental in ensuring the continuation of this project. The authors also want to acknowledge the technical support and contribution from the following TxDOT personnel: Doug Eichorst, Magdy Mikhail, Caroline Heinen, Joe Leidy, Darlene Goehl, and Robin Hwang.

Table of Contents

List of Figures

List of Tables

Chapter 1. Project Plan and Work Plan for Task Order No. 1

1.1 Background

Various overlay materials and preservation techniques are available to extend the service life of pavements in Texas. These techniques include thin overlays, chip seals, micro-surfacing, ultra-thin friction course, slurry seals, cape seals, scrub seals, etc. While some of these are interim measures applied as stop-gaps before full rehabilitation, others are designed to provide extended service lives. This is the case with the thin overlays that have been gaining popularity in recent years due to budget constraints. In contrast to conventional rehabilitation strategies using thicker traditional overlay, thin overlay and other preservation techniques are used on existing pavements to extend their remaining life. Therefore, pavements resurfaced using these techniques will be subject to the pre-existing failure mechanisms of the underlying pavement, which may serve to accelerate deterioration and reduce the effectiveness of these techniques. The rate of deterioration of these thin overlays and other alternative treatments will vary depending on the condition or state of the underlying pavement as well as other factors, including the quality of the treatment applied (type of treatment and material properties) and external influences such as traffic (in terms of volume, axle loads, and speed) and climate (temperature and rainfall).

Thus, research is needed to provide a better understanding of the effectiveness of thin overlays (such as ultra-thin overlay mixes, bonded wearing courses, crack-attenuating mixes, and ultra-thin porous friction courses) relative to other preservation techniques (such as seal coats, slurry seals, and micro-surfacing) and the impacts of the various influence factors. An increased understanding will help optimize the application of preservation techniques and provide proper quantification of the expected lives of various treatments under different operating conditions.

1.2 Scope and Objective

The objective of this project is to quantify the *field performance* of thin overlays relative to various other popular preservation treatments under varying pavement, traffic, and climate conditions, with an eye towards optimizing the design and application of these treatments in Texas.

1.3 Work Plan

The following tasks have been identified as a general framework for completion of this research:

Task 1: Information Gathering

Conduct a literature review and survey local and state authorities on the use of thin overlay and other comparable preservation techniques with the goal of establishing the current state of practice. This review and survey will address the design, construction, application, and performance of these techniques. Attention will be given to types of materials used for the different overlays in terms of aggregates, binders, and additives as well as the timing of these overlays. Special consideration must be given to the various influences impacting the rate of deterioration of preventive maintenance treatments to allow identification of the most significant factors influencing service life. The review must also identify the various measures used to quantify the performance of thin overlays and alternative treatments.

Task 2: Experimental Design

Based on Task 1, develop an experimental design to test the most used thin overlays in Texas and comparable preservation treatments applied by local and state authorities, addressing all significant influence factors in terms of the pre-existing condition of the underlying pavement, quality of the treatment applied, traffic (in terms of volume, axle loads, and speed) and climate (in terms of temperature and rainfall). The experimental design must account for replication of influence factors and be robust enough to address a broad spectrum of applications but flexible enough to allow practical application thereof. Thereafter, field sections recently constructed in the various districts in Texas will be identified and selected for further monitoring and evaluation.

Task 3: Identification of Field Sections

Identify roadway sections with various types of thin overlays and other comparable preservation treatments that match the conditions and limits of the experimental design levels developed in Task 2. It is anticipated that various sections throughout Texas will be selected, particularly in those TxDOT Districts that are extensively applying thin overlays. Prepare a detailed experimental plan to measure the performance response of the identified sections outlining logistical details, allowing repeated monitoring of the sections over a two-year period. This plan must include the identification of control sections for feasible comparisons.

Task 4: Performance Monitoring and Evaluation

Execute the experimental plan developed in Task 3, including the collection of performance measures of both the experimental and control sections as well as accurate assessments of prevailing traffic and climate conditions in these sections. Sufficient performance measurements must be obtained to allow the development of performance trends and early deterioration models.

In addition to the visual assessment of the sections to monitor structural distresses such as cracking and rutting, emphasis will be placed on measuring the functional performance of the sections in terms of roughness, macro-texture, and skid resistance. Noise testing of the sections using the onboard sound intensity equipment is also an option. Thin overlays are especially sensitive to the performance of the underlying pavement structure. Thus, assessing the bearing capacity using a falling weight deflectometer and dynamic cone penetrometer will be beneficial. In addition, the response of the thin overlays will be monitored for shoving and debonding, raveling and stone loss, edge-breaks, and other surface distresses, such as potholes.

To effectively track the performance of the experimental and control sections, the research team will need to identify and monitor all preventive maintenance measures applied to ensure that these are adjudicated fairly and will not bias the experiment.

Task 5: Data Analysis and Comparison

Apply statistical techniques to evaluate the performance of the sections measured in Task 4 towards establishing the expected lives of thin overlays in Texas relative to various treatments under different operating conditions. Demonstrate application of the findings to establish the benefit:cost ratio of the experimental sections compared to the control sections. This analysis will include the cost of preventive maintenance measures applied to the respective sections over the analysis period.

Task 6: Preparation of Recommendations and Study Report

Document the research undertaken as part of the project in a final report that provides recommendations to properly quantify the expected lives of various treatments under different operating conditions.

1.4 Deliverables

This project's deliverables will consist of a final report that documents the research undertaken as part of the project and that provides recommendations to properly quantify the expected lives of various thin overlays in Texas and other preservation treatments under different operating conditions.

1.5 Project Budget and Duration

- Estimated Project Initiation: 1st March 2015
- Estimated Project Completion: 28th February 2017
- Total Estimated Budget: $261,763 for 24 months

It should be noted that this amount includes $98,000 for the purchase of a grip tester to assess the field performance of thin overlays in terms of skid resistance.

1.6 Implementation Significance

The implementation of the findings of this project will allow the establishment of the benefit:cost ratio of various thin overlays relative to comparable preservation treatments and will provide a sound engineering basis for the selection of the right treatment for the right road at the right time.

Chapter 2. Project Plan and Work Plan for Task Order No. 2

2.1 Background

The effect of the aggregate texture (micro-texture) and the effect of the texture of the compacted hot-mix asphalt (macro-texture) on the skid resistance of a highway surface are well recognized. However, we lack a fundamental understanding of the individual effect that each of these two properties, micro- and macro-texture, have on the final skid properties of the road. Most research studies in this area have been based on theory, assumptions, and sound engineering judgment. The individual effects have not been quantified and their contributions to skid under varying levels of moisture, speed, and highway condition are not well understood. Recent developments in optics and computers have allowed the collection of high definition 3-D images of the surface of the highway pavement. In particular, it is now possible to quantify micro-texture in the field in an effective and efficient manner. This can be done with the use of laser-based technology that allows measurements below 0.5 mm. Locally, the Texas A&M Transportation Institute (TTI) has conducted research using the Aggregate Imaging System (AIMS) to evaluate aggregate properties and to establish relationships with skid. The AIMS combines hardware that captures real-time digital images of paving material samples, and software that analyzes shape, texture and ratio characteristics of aggregates. The AIMS is, however, an optical instrument whose resolution does not allow the accurate quantification of micro-texture to the extent that laser does. Nevertheless, this project offers a unique opportunity to compare the findings of both studies and gain mutual benefit by evaluating the same sections and materials with both technologies and establishing meaningful comparisons.

2.2 Scope and Objective

During this study, we will apply 3-D laser technology to quantify the micro-texture and macro-texture of different pavement surfaces and determine their skid characteristics. We will use a new model laser texture scanner. Through posterior panel data analyses of the information, we will investigate the relative contribution of micro- and macro-texture to skid resistance in the field and develop guidelines for aggregate and mix selection for improved long-term skid. We will carry out field measurements in some of the same sections as the recently completed TTI study to continue to improve on the prediction of skid based on texture measurements.

2.3 Work Plan

Task 1: State of the Art

During this task we will conduct an extensive international literature search to determine the state of the practice and the state of the art in terms of field measurement of micro- and macro-texture. The literature review will also focus on identifying theory and models that relate micro- and macro-texture measurements to skid resistance at various speeds and under different conditions (e.g., dry and wet surface, smooth and rough pavement, etc.). We will also evaluate the properties and measurements performed by the AIMS as they compare with equivalent laser measurements.

Task 2: Development of Experiment and Field Testing

During this task and based on the information collected during Task 1, we will develop a field experiment that will consist of a series of field test sections where we will be measuring micro- and macro-texture as well as skid using different equipment and under different conditions. Some of the conditions to investigate as part of the study will include:

- Dry and wet pavement surface.
- Variable characteristic speed.
- Asphalt mixes and seal coats of different maximum aggregate sizes.
- Aggregates with different texture and surface hardness (abrasion characteristics and durability).
- Trafficked (wheelpath) and untrafficked (between) sections.
- Other relevant conditions as identified in Task 1.

These sections will be primarily selected for the experiment conducted during the study by TTI so that both projects will benefit from the data and findings. It is anticipated that approximately 16 field sections will be monitored—ideally, all of them from the TTI study unless we find gaps in the experimental design that will require additional sections with particular characteristics or conditions as listed above.

Task 3: Data Analysis

During this task we will conduct a detailed and comprehensive analysis of the data collected during Task 2. Two types of analyses will be conducted: 1) power spectral density (PSD) analysis and 2) empirical evaluation by applying advanced panel data analysis. The objective of these analyses is to determine the frequency components that are correlated with aggregates, surface profiles, and mixtures that offer higher skid resistance. This information will serve as the basis for the development of the guidelines.

The initial literature review indicated that other, more complex techniques could also be appropriate, such as wavelet analysis and Monte Carlo simulations. However, the more theoretical studies in terms of data analysis are being conducted by the research team as part of a federal grant supplied by the U.S. Department of Transportation. TxDOT funds for this project will primarily be used for the field component of the study.

Task 4: Implementation and Technology Transfer

During this final task we will prepare a research report documenting all work performed under the various tasks, the experimental design, the data collected, the data analyses, and the methodologies applied. An appendix to this research report will contain the guidelines for the selection of aggregate and mix type to enhance skid resistance. The research will also be summarized in a conference paper that will be submitted to the Annual Meeting of the Transportation Research Board and in a journal article to be submitted to a relevant refereed technical journal. We will also report on the comparison between the AIMS-measured properties and those produced by the analysis of the laser-based measurements.

2.4 Project Deliverables

- Research report that documents all work performed.
- Database containing all experimental data.
- Guidelines for the selection of aggregate and mix type for improving skid resistance efficiency.
- Comparison between AIMS and laser-based measurements.
- A journal article and a conference paper that summarize the main findings and recommendations of the research.

2.5 Cost and Duration

- Estimated Project Initiation: 1st March 2015
- Estimated Project Termination: 31st August 2016 (18 months)
- Estimated Total Budget: $209,570 (including $76,000 for the purchase of a dynamic friction tester and a circular tester meter to measure texture and friction in the field). The research team already owns a Model 9200 Laser Texture Scanner with a vertical sample resolution of 0.015 mm and horizontal sample spacing of 0.015 mm, which will enable us to accurately quantify micro-texture.

2.6 Implementation Significance

The implementation of the findings of this research will provide TxDOT with a methodology and guidelines for a more efficient determination of the skid conditions of their highway network, thus identifying potentially unsafe segments requiring corrective actions—allowing proactive response and minimizing the potential for accidents. Current methods for determining skid resistance directly are slow and inefficient.

Chapter 3. Progress to Date on Task Order No. 1: Determination of Field Performance of Thin Overlays Relative to Alternative Preservation Techniques

3.1 Preliminary Analysis using LTPP SPS-3 Data

This chapter documents the preliminary analysis performed to quantify the effectiveness of different preventive maintenance (PM) treatments through a model-based approach using pavement sections included in the Specific Pavement Study (SPS)-3 experiment of the Federal Highway Administration (FHWA) Long-Term Pavement Performance (LTPP) program. The models developed as part of this task, along with other statistical techniques, will be adapted for the analysis of performance of thin overlays relative to alternative preservation techniques of actual field pavement sections from the TxDOT highway network.

3.2 Introduction

The ever-decreasing funding levels for managing the highway network highlight the need for optimizing maintenance and rehabilitation strategies in order to delay damage and preserve the value of the infrastructure assets. A number of PM treatments are available specifically to extend the service life of pavements. These techniques include crack seals, thin overlays, chip seals, micro-surfacing, cold in-place recycling, ultra-thin friction course, fog seals, slurry seals, cape seals, and scrub seals. While some of these are interim measures applied as stop-gaps before full rehabilitation, others are designed to provide extended service life. In contrast to conventional rehabilitation strategies, PM treatments are used on existing pavements with reduced remaining life. Therefore, these treatments will be subject to the pre-existing failure mechanisms of the underlying pavement, which may serve to accelerate deterioration and reduce the effectiveness of the PM treatment. The rate of deterioration of these treatments will vary depending on the condition or state of the underlying pavement but also other factors including the quality of the treatment applied and external influences with regards to traffic and climate. For this reason, research is needed to provide a better understanding of the effectiveness of different PM techniques and how these are impacted by different influence factors.

The objective of this study is to quantify the expected lives of various popular PM treatments under varying pavement, traffic, and climate conditions with the goal of optimizing the design and application of these treatments. The effectiveness of the different PM treatments will be assessed and ranked through the statistical analysis and modelling of the performance response of a set of treated and non-treated (control) pavement sections representative of Texas highway conditions. The pavement sections for the analyses will be selected in order to address replication of all influence factors in terms of the pre-existing condition of the underlying pavement, quality of the treatment applied, traffic (in terms of volume, axle loads, and speed) and climate (in terms of temperature and rainfall). The proposed approach will require the development of a database containing relevant design, construction, application, and performance data of the selected PM treatments. This database will be developed from processing and merging a number of existing databases extracted from different TxDOT's information systems, such as the Design and Construction Information System (DCIS), SiteManager, the Maintenance Management Information System (MMIS), and the Pavement Management Information System (PMIS). In

addition, the analysis of this study will include experimental pavement sections from the FHWA's LTPP program. LTPP data consists of high-quality, detailed measurements taken for a controlled experiment that includes pavement sections treated with different PM techniques. Therefore, this data is fit for developing and checking the performance models to be used for analyzing the Texas pavement data.

This chapter documents the preliminary analysis performed using LTPP data to quantify the effectiveness of PM treatments through a model-based approach. The proposed model aimed to explain the relationship between the loss in serviceability rate as a function of treatment type along with pavement, traffic, and climate conditions as well as their interaction with the PM treatment's effectiveness. The models presented will be adapted and estimated using TxDOT data once the processing of the aforementioned databases is completed.

3.3 Background

The LTPP program included an SPS-3 experiment designed to assess the effectiveness of PM treatments on flexible pavements and to evaluate the optimum timing to apply the treatments. The SPS-3 experiment considered four different PM treatments: thin hot-mix asphalt overlay (**TH**), slurry seal (**SS**), chip seal (**CH**), and crack seal (**CS**). These PM treatments were applied to consecutive sections of the road along with non-treated (control) sections at 81 sites located in the United States and Canada during the early 1990s. Thus, each site consisted of five consecutive sections all subjected to the same traffic loads, structure, and environmental conditions. Some of the experimental design factors considered for the SPS-3 experiment included four climatic regions and two subgrade types; however, the combinations of treatments were not considered.

A number of studies have used data from the LTPP SPS-3 experiment to assess the effectiveness of PM treatments, adopting different performance indices and implementing methodologies that included multiple regression analysis (Morian et al., 1998), survival analysis (Eltahan et al., 1999; Morian et al., 2011), and various statistical comparison techniques (Hall et al., 2003; Shirazi et al., 2010; Morian et al., 2011). Although the previous studies provide information on the relative effectiveness of treatments, the authors believe that the use of a regression analysis to develop a model can be further explored.

The preliminary analysis presented in this chapter quantifies the effectiveness of PM treatments through a model-based approach using censored regression. The proposed approach overcomes limitations from previous studies in that it allows for comparing the treatment effectiveness for a particular experimental factor while controlling for the remaining factors, producing more robust estimates of the treatment marginal effect. In addition, the proposed model specification accounts for more variables and more realistic assumptions than previous regression analyses found in the literature.

3.4 Literature Review

In 1998, Morian et al. applied multi-variable regression analysis to 5-year SPS-3 data to evaluate the PM treatment performance. This study modeled different performance indicators in terms of treatment type, environmental zone, age, and initial condition, among other factors. In the regression analysis, the independent variables were specified as integer indicator codes ranked from worst to best. The study concluded that TH significantly reduced rutting and roughness while the remaining PM treatments had slight or no effect. However, the researchers' assumptions about the rank of each independent variable resulted in biased parameters, not capturing the true marginal effects of the different PM treatments.

One year later, Eltahan et al. (1999) conducted survival analysis to evaluate the life expectancy and the effect of the original pavement condition. The authors estimated the failure probabilities of each treatment with respect to the original condition of the test sections using the Kaplan-Meier method. The study concluded that applying treatment to sections in poor condition increased the risk of failure by two to four times, and that CH outperformed the other four treatments.

In 2003, Hall et al. evaluated the initial and long-term effect of the different PM treatments on the pavement condition as well as the influence of pre-treatment condition and other experimental factors. The treatment initial effect was evaluated by comparing pre- and post-treatment measurements of roughness, rutting, and fatigue cracking, whereas the long-term effect was evaluated by comparing the last measurements of the treated and control sections. The comparisons were carried out using two-sided multiple comparisons with the control section and paired t-tests. The study concluded that the most effective treatment in the SPS-3 experiment was TH, followed by CS and SS, and that only TH produced an initial reduction as well as a significant long-term effect on roughness.

Another study conducted in 2003 by Chen et al. studied 14 SPS-3 test sites in Texas to investigate the effectiveness of PM treatments. The study concluded that CH was the best performer among the four analyzed PM treatments, followed by TH. Although the study presents a detailed discussion of the PM treatment effects on Texas specific sites, the results from the comparison were not based on statistical methods. In addition, factors such as subgrade type, moisture, and temperature were not taken into account.

In 2010, Shirazi et al. used Friedman tests and non-parametric randomized block analysis of variance to compare the performance of the different PM treatments for different levels of temperature, precipitation, subgrade, traffic, and initial condition. The performance indicator used in this study was computed as the weighted average of distresses normalized by the period of analysis. This indicator allowed for comparing between different data collection periods; however, it did not take into account the deterioration rate and its trend. The study concluded that TH was the most effective treatment whereas the effect of SS and CS was not statistically significant.

A more recent study in 2011 conducted by Morian et al. applied survival analysis to 20-year SPS-3 data to assess life expectancy of the PM treatments, along with Friedman test to compare structural effects of the treatments. The results from the survival analysis indicated that TH performed best at high survival probabilities, whereas CH performed best for the case of low survival probabilities. The Friedman test results showed that the structural benefits from all treatments (except for CS) were significant.

Lastly, Haider and Dwaikat (2011) estimated the optimum timing for PM treatment by maximizing the difference between the areas below the roughness curves for pre- and post-treated pavements. The International Roughness Index (IRI) value was modeled as a function of age using an exponential function. The effects of traffic, environmental, and subgrade factors were not taken into account in the analyses, and the study did not include a comparison between treatments.

3.5 Description of Damage Rate Model and Data

3.5.1 Damage Rate Model Specification

The main goal of developing a pavement damage rate (DR) model is two-fold: 1) to accurately predict the damage of a pavement section between data collection periods; and 2) to unveil the underlying intricate relationships between the pavement properties and the DR, which

will allow for quantifying the effect of the different PM treatments. The pavement DR was defined as the loss in serviceability per unit traffic, and it was computed as the ratio between the change in IRI value and the increment in traffic demand observed between data collection dates, as expressed in Eq. 3.1.

$$DR_{i,\Delta t} = \Delta IRI_{i,\Delta t} / \Delta N_{i,\Delta t} \quad (3.1)$$

Where:
$DR_{i,\Delta t}$: Damage rate for section i and period of analysis Δt, in m/km/kESAL
$\Delta IRI_{i,\Delta t}$: Change in IRI, in m/km
$\Delta N_{i,\Delta t}$: Increment in traffic, in kESAL
i: sub-index to indicate pavement section number
Δt: sub-index to indicate period of analysis, between roughness data collection dates

The DR model in this study was specified as a linear combination of a number of explanatory variables that included the PM treatment types as well as structural, environmental, and traffic factors. The variables selected to explain the pavement DR are presented in Eq. 3.2. A variable for temperature was not included in the model specification in order to avoid multi-collinearity issues due to its high correlation with the freezing index in the used dataset.

$$\boldsymbol{X}_{i,\Delta t} = \left[TH_i, CH_i, SS_i, CS_i, AC_i, BA_i, SB_i, SG_i, \log\left(N_{i,\Delta t}\right), FrInd_i, Precip_i, PreDam_i\right] \quad (3.2)$$

Where:
$\boldsymbol{X}_{i,\Delta t}$: Vector of explanatory variables
TH: Application of Thin Overlay, equal to 1 for TH treatment and 0 otherwise
CH: Application of Chip Seal, equal to 1 for CH treatment and 0 otherwise
SS: Application of Slurry Seal, equal to 1 for SS treatment and 0 otherwise
CS: Application of Crack Seal, equal to 1 for CS treatment and 0 otherwise
AC_i: Total thickness of asphalt layers, in mm
BA_i: Total thickness of base layers, in mm
SB_i: Total thickness of sub-base layers, in mm
SG_i: Sub-grade type, equal to 0 for fine soil and 1 for coarse soil
$N_{i,\Delta t}$: Cumulated traffic until the period of analysis Δt, in kESAL
$FrInd_i$: Annual Average Freezing Index, in degrees Celsius (°C) degree-days
$Precip_i$: Annual Average Precipitation, in mm
$PreDam_i$: Measured IRI value of the section when the treatment was applied, in m/km.

The explanatory variables related to cumulated traffic, or age, were log-transformed, allowing, thus, for non-linear relationship between DR and time. Furthermore, it should be noted from Eq. 3.1 that DR is the first derivative of the roughness curve with respect to traffic for the case of an infinitesimal period of analysis. Therefore, the proposed DR linear model specification captures the observed non-linear trend of the pavement serviceability curve as a function of traffic, while allowing for the analytical convenience of estimating a linear model.

Censored Regression Model

Theoretically, DR is a non-negative random variable given that pavement roughness is expected to either increase or remain constant as a function of traffic. Therefore, the DR values computed from the data were censored allowing only for positive values; i.e., censoring the observations for which the roughness decreased after the pavement was subjected to traffic loads for a period of time. The observed negative change in roughness between data collection periods is explained, in part, by measuring equipment error.

The large portion of censored DR values corresponding to data points with no significant change in serviceability observed in the data invalidates the conventional regression assumptions and would result in biased ordinary least squares estimates. In order to properly account for the censored values, DR was modelled adopting a type I Tobit model structure. This model structure is a particular case of censored regression, which is typically used for handling dependent variables dominated by a particular response (in this case, zeros). A standard Type I Tobit specification for our DR model is described in Eq. 3.3a to 3.3c (Wooldridge, 2010).

$$DR_{i,\Delta t} = \max\left(0, DR^*_{i,\Delta t}\right) \tag{3.3a}$$

$$DR^*_{i,\Delta t} = \boldsymbol{X}'_{i,\Delta t}\boldsymbol{\beta} + u_{i,\Delta t} \tag{3.3b}$$

$$u_{i,\Delta t} \sim \text{Normal}(0, \sigma^2) \tag{3.3c}$$

Where:
DR^*_i: Latent damage rate
$\boldsymbol{X}_{i,\Delta t}$: Vector of explanatory variables
$\boldsymbol{\beta}$: Vector of regression coefficients
$u_{i,\Delta t}$: Idiosyncratic error term
σ: Standard deviation of the error term

The Tobit model is similar to a linear regression model except that the model recognizes the dichotomization of the dependent variable into zero and non-zero sets. This model allows for estimating the probability of a pavement section to exhibit zero roughness change, which is useful to identifying the factors that contribute to maintain the pavement serviceability fairly unchanged for a period of time. Moreover, the estimated regression parameters corresponding to the explanatory variables will be unbiased.

The predicted DR for a particular pavement section i and period time Δt is given by the expected value of the DR for a given set of explanatory variables, and estimated as in Eq. 3.4. In addition, the probability of a pavement section to remain unchanged in terms of IRI is computed as in Eq. 3.5.

$$\text{E}\left(DR_{i,\Delta t} | \boldsymbol{X}_{i,\Delta t}\right) = \Phi\left(\frac{\boldsymbol{X}'_{i,\Delta t}\boldsymbol{\beta}}{\sigma}\right)\boldsymbol{X}'_i\boldsymbol{\beta} + \sigma\phi\left(\frac{\boldsymbol{X}'_{i,\Delta t}\boldsymbol{\beta}}{\sigma}\right) \tag{3.4}$$

$$\text{P}\left(DR_{i,\Delta t} = 0 \middle| \boldsymbol{X}_{i,\Delta t}\right) = 1 - \Phi\left(\frac{\boldsymbol{X}'_{i,\Delta t}\boldsymbol{\beta}}{\sigma}\right) \tag{3.5}$$

Where:
$\phi(\cdot)$: Probability density function of standard normal distribution
$\Phi(\cdot)$: Cumulative distribution function of the standard normal distribution

As observed from Eq. 3.4, the explanatory variables are non-linearly related to the DR prediction; thereby the interpretation of the regression parameters, $\boldsymbol{\beta}$, is not straightforward. We used econometric elasticity to examine the sensitivity of explanatory variables on the pavement DR. Econometric elasticity, or marginal effect (for indicator variables), is defined as the change in the explained value per unit change in the explanatory variable while keeping the remaining variables fixed. Eq. 3.6 was used to estimate the econometric elasticity of a continuous variable x_j, whereas Eq. 3.7 was used to estimate the marginal effect of a binary variable x_r.

$$\frac{\partial E(DR|\boldsymbol{X})}{\partial x_j} = \Phi\left(\frac{\boldsymbol{X'\beta}}{\sigma}\right)\beta_j \tag{3.6}$$

$$\frac{\partial E(DR|\boldsymbol{X})}{\partial x_r} = \frac{\mathrm{E}\left(DR_{i,\Delta t}|(X_1,\ldots,X_r=1,\ldots,X_n)\right)-\mathrm{E}\left(DR_{i,\Delta t}|(X_1,\ldots,X_r=0,\ldots,X_n)\right)}{1-0} \tag{3.7}$$

Both the magnitude and the corresponding standard errors of the aforementioned Tobit model parameters were obtained through maximum likelihood estimation (MLE) using R programming language (R Core Team, 2014) employing AER package (Kleiber and Zeileis, 2015). A final specification was chosen carefully based on a rigorous model development process. Model refinement was carried out through exclusion of statistically insignificant variables by following standard step-wise procedures and statistical tests (e.g., F-test). Practical considerations played a role in the removal of insignificant variables, rather than solely adopting a statistics-based mechanical approach. The results from the proposed Tobit regression model is presented in the following section of the chapter.

3.6 Processing of LTPP SPS-3 Dataset

The data used for estimating the proposed DR censored regression model was collected for the LTPP SPS-3 experiment, and obtained from the Standard Data Release version 29 (LTPP InfoPave, 2015). The main filtering criteria applied to the original dataset consisted of considering only the pavement sections containing at least one computed annual number of ESAL during the years for which the SPS-3 experiment was conducted. The computed annual number of ESAL was obtained from the "TRF_ESAL_COMPUTED" table, and was estimated from monitored axle data (Elkins et al., 2003). Traffic data estimated from other sources were filtered out in order to make use only of the best quality of data available for estimating the model.

The change in IRI values, $\Delta IRI_{i,\Delta t}$ (Eq. 3.1), was computed as the difference between consecutive IRI measurements. Therefore, only sections with at least two roughness measurements collected during the SPS-3 experiment were considered for the study. The resulting dataset after applying the two mentioned filters included data at 64 SPS-3 sites (each site containing multiple pavement sections), shown in Figure 3.1, representing different climatic regions.

Figure 3.1: Location of LTPP SPS3 sections used in the study

In addition, the increments in traffic values, $\Delta N_{i,\Delta t}$ (Eq. 3.1), were estimated as the sum of all annual ESALs (equivalent single axle load) corresponding to section i, weighted by the proportion of time falling within the period of analysis Δt. The annual ESALs for the years with missing traffic data were estimated as the mean of the set of computed annual ESALs for the corresponding section.

Lastly, the values for the cumulated traffic until the period of analysis, $N_{i,\Delta t}$ (Eq. 3.2), were computed as the sum of all preceding increments of traffic ($\Delta N_{i,\Delta t}$) for the corresponding pavement section. The remaining explanatory variables from Eq. 3.2 were extracted from the original dataset without further processing.

3.7 Results from Estimation of DR Models

3.7.1 PM Treatments Marginal Effects

The model proposed for assessing the effectiveness of PM treatments followed the Tobit model structure presented in Eq. 3.3, with the latent DR specified as in Eq. 3.8; where the pavement DR is expressed as a function of the PM treatment type along with structural, environmental and traffic variables. Thus, the DR model is able to properly handle the significant portion of zero (censored) values in the distribution of the dependent variable, and it allows for estimating the marginal effect of the different treatments while accounting for multiple experimental variables simultaneously.

$$DR^{*}_{i,\Delta t} = \beta_0 + \beta_{AC}AC_i + \beta_{BA}BA_i + \beta_{SB}SB_i + \beta_{SG}SG_i + \beta_{logN}\log(N_{i,t}) + \beta_{logN}\log(N_{i,t}) + \beta_{FrInd}FrInd_i + \beta_{Precip}Precip_i + \beta_{TH}TH_i + \beta_{CH}CH_i + \beta_{SS}SS_i + \beta_{CS}CS_i + u_{i,\Delta t} \quad (3.8)$$

The model in Eq. 3.8 was specified without interaction terms and using the control sections as the base; therefore, it was used to quantify the global marginal effect of the PM treatments with respect to non-treated pavements. The marginal effects for each treatment was quantified as in Eq. 3.7, using the estimated parameters of the model and fixing the remaining variables at their mean value. In addition, the model specification was modified and estimated using the different treatments as the base indicator variables one at a time, in order to rank the effectiveness of the different treatment strategies.

The estimated PM treatments marginal effects are presented in the columns of Table 3.1, where each column corresponds to the models using the different indicator variables as the base. The negative sign on the marginal effect of every PM treatment relative to the control sections indicates that all of the treatment had, in average, a smaller DR than non-treated sections. Therefore, all treatments helped to slow down the loss in serviceability for any given combination of cumulated traffic, environmental and structural factors.

The results from the models using the different treatment as the base allow to perform pair-wise comparisons between the effectiveness of each pair of treatments and, therefore, to rank the four PM treatment from most to least effective. From the comparison among the different treatments, none of the marginal effects were statistically significant (represented with a zero value in Table 3.1). Therefore, although all PM treatment were superior to non-treated sections, there was not enough evidence to determine what treatment was the most effective. Despite the statistically insignificant differences among the four treatments' effectiveness, the first column of Table 3.1 suggest that TH and CH were more efficient than SS and CS, TH being the most efficient treatment.

The marginal effects from Table 3.1 can be used to estimate the expected difference in IRI for a given increment in traffic, ΔN; e.g., for the median annual increment of traffic in the dataset, 79 kESAL per year, a pavement section treated with a thin overlay would present 0.43 m/km (27 in/mile) less IRI after five years of constant traffic than if the section had not been treated. Clearly, the beneficial impact of applying the treatment will be more noticeable for sections with higher traffic levels and longer period of analysis.

Table 3.1: Marginal effect of PM treatments for the global model in Eq. 3.8 using different base treatments

	Marginal Effect of PM Treatment [m/km/kESAL]				
	base = Co	*base = TH*	*base = CH*	*base = SS*	*base = CS*
Co	-	1.10E-03	0.96E-03	0.67E-03	0.79E-03
TH	-1.10E-03	-	0.00	0.00	0.00
CH	-0.96E-03	0.00	-	0.00	0.00
SS	-0.67E-03	0.00	0.00	-	0.00
CS	-0.79E-03	0.00	0.00	0.00	-

3.7.2 Impact of Preexisting Damage and Environmental Factors on PM Treatments Effectiveness

The next step consisted of evaluating what variables in our dataset affect the effectiveness of the PM treatments in order to determine the optimal conditions for treating the pavement. For this, the latent DR variable from the Tobit model used to study the global marginal effects of the PM treatments (Eq. 3.8) was modified by adding interaction terms to the treatment indicator variables as shown in Eq. 3.9. The $PreDam_i$ variable incorporated into the new specification consists of the measured IRI value of the section when the treatment was applied and it is an indicator of the preexisting damage of the pavement. The main effect of the preexisting damage variable was not included in the model since it is not defined for the case of non-treated sections. Therefore, the new specification allowed for quantifying the effectiveness of each PM treatment as a function of the section's freezing index, precipitation and preexisting damage, and it was estimated using censored regression.

$$
\begin{aligned}
DR^{*}_{i,\Delta t} = {} & \beta_0 + \beta_{AC}AC_i + \beta_{BA}BA_i + \beta_{SB}SB_i + \beta_{SG}SG_i + \beta_{logN}\log\left(N_{i,t}\right) + \\
& \beta_{FrInd}FrInd_i + \beta_{Precip}Precip_i + \beta_{TH}TH_i + \beta_{CH}CH_i + \beta_{SS}SS_i + \beta_{CS}CS_i + \\
& TH_i\left[\beta_{TH} + \beta_{TH.FrInd}FrInd_i + \beta_{TH.InDam}PreDam_i + \beta_{TH.Precip}Precip_i\right] + \\
& CH_i\left[\beta_{CH} + \beta_{CH.FrInd}FrInd_i + \beta_{CH.InDam}PreDam_i + \beta_{CH.Precip}Precip_i\right] + \\
& CS_i\left[\beta_{CS} + \beta_{CS.FrInd}FrInd_i + \beta_{CS.InDam}PreDam_i + \beta_{CS.Precip}Precip_i\right] + \\
& SS_i\left[\beta_{SS} + \beta_{SS.FrInd}FrInd_i + \beta_{SS.InDam}PreDam_i + \beta_{SS.Precip}Precip_i\right] + u_{i,\Delta t}
\end{aligned}
\tag{3.9}
$$

Table 3.2 presents the MLE estimates, the p-values, and the mean elasticity of the parameters with a significant effect on the pavement DR. The parameters in Eq. 3.9 not included in Table 3.2 were not statistically significant and therefore removed from the final model specification, except for the parameters β_{SG} and $\beta_{CS.PreDam}$. The results show that neither the main effect of the section's freezing index nor its interaction with any of the PM treatments were statistically significant. Furthermore, the main effect of the precipitation variable was also not significant, indicating that the section's annual mean precipitation does not have a significant effect on the control sections; however, data suggests that precipitation affects the effectiveness of the PM treatments.

The effect of the structural layer thicknesses and their relative importance were as expected. A statistically significant negative effect suggests that thicker layers are associated with slower deterioration of the pavement. The effect of the asphalt layer thickness was the greatest, followed by the base thickness. The negative sign of the parameter on the subgrade variable reflects the slower DR of coarse subgrade relative to finer, and the expected difference is quantified by its marginal effect, equal to -7.70E-04 m/km/kESAL. Finally, the parameter on the log of the cumulated traffic, which accounts for the effect of the pavement age, was negative and statistically significant. Therefore, the relationship between roughness and traffic demand was non-linear and the pavement DR decreases with time.

Regarding the interaction parameters of the model, it is observed that both the section's preexisting damage and annual mean precipitation affected the effectiveness of the PM treatment, as measured by the difference in DR relative to the non-treated sections. The positive sign of the parameters on the interaction terms between PM treatments and pavement preexisting damage indicates that PM treatment effectiveness decreases with the increase of initial IRI value. Therefore, the PM treatments were more effective when applied on sections with less preexisting

damage. This observation reinforces the main purpose of applying PM, which is not to add structural capacity to the pavement but to delay the structural failure. Furthermore, the effectiveness of CH and CS were less affected by the preexisting condition than for TH and SS treatments. Lastly, the negative sign of the parameters on the interaction terms between PM treatments and the precipitation variable indicates that all the PM treatments were more effective when applied on sections with higher mean annual precipitation. This observation suggests the importance of the surface sealing provided by the PM treatments, which reduces the weakening of the pavement structure due to the presence of water, thereby slowing down the pavement DR.

Table 3.2: MLE estimates, p-value and mean elasticities of parameters from the model with interactions (Eq. 3.9)

	coeff	***p-value***	***elasticity***
$\boldsymbol{\beta_0}$	1.30E-02	0.000	-
$\boldsymbol{\beta_{AC}}$	-7.31E-06	0.041	-1.00E-04
$\boldsymbol{\beta_{BA}}$	-6.39E-06	0.006	-8.74E-05
$\boldsymbol{\beta_{SB}}$	-4.13E-06	0.003	-5.64E-05
$\boldsymbol{\beta_{SG}}$	-8.14E-04	0.129	-7.70E-04
$\boldsymbol{\beta_{logN}}$	-1.43E-03	0.000	-1.00E-04
$\boldsymbol{\beta_{TH.PreDam}}$	2.30E-03	0.045	1.16E-03
$\boldsymbol{\beta_{CH.PreDam}}$	1.03E-03	0.053	5.64E-04
$\boldsymbol{\beta_{SS.PreDam}}$	2.04E-03	0.005	1.10E-03
$\boldsymbol{\beta_{CS.PreDam}}$	1.00E-03	0.190	5.50E-04
$\boldsymbol{\beta_{TH.Precip}}$	-5.49E-06	0.000	-2.78E-06
$\boldsymbol{\beta_{CH.Precip}}$	-3.82E-06	0.000	-2.08E-06
$\boldsymbol{\beta_{SS.Precip}}$	-4.92E-06	0.000	-2.65E-06
$\boldsymbol{\beta_{CS.Precip}}$	-2.98E-06	0.038	-1.63E-06

The effects of the section's preexisting damage and annual mean precipitation on the PM treatment effectiveness are illustrated in Figure 3.2 and 3.3. The predicted IRI values for a pavement section with mean structural and environmental conditions and fine subgrade were calculated as in Eq. 3.10, derived from Eq. 3.1 and 3.4.

$$\widehat{IRI}_{\mathrm{t}} = IRI_0 + \sum_0^t E[DR_{\Delta t}|\boldsymbol{X}]\Delta N_{\Delta t} = IRI_0 + \sum_0^t \left[\Phi\left(\overline{\boldsymbol{X}}'_{\Delta t}\widehat{\boldsymbol{\beta}}/\hat{\sigma}\right)\widehat{\boldsymbol{X}}'_{\Delta t}\widehat{\boldsymbol{\beta}} + \sigma\phi\left(\overline{\boldsymbol{X}}'_{\Delta t}\widehat{\boldsymbol{\beta}}/\hat{\sigma}\right)\right]\Delta N_{\Delta t} \quad (3.10)$$

Where:
$\widehat{IRI}_{\mathrm{t}}$: Predicted IRI value at time t,
IRI_0: Initial IRI value

$\bar{\boldsymbol{X}}_{\Delta t}$: Explanatory variables set to the cumulated traffic for the period of analysis, fine subgrade and mean values for the remaining variables.
$\widehat{\boldsymbol{\beta}}$: MLE estimates (Table 3.2) from censored regression of model with interactions
$\hat{\sigma}$: Estimated standard deviation of the model's error term

Figure 3.2 shows the predicted IRI curves corresponding to each PM treatment and control for two levels of mean annual precipitation: the 75th (solid lines) and the 25th (dashed lines) percentiles. All other explanatory variables were fixed to their mean value and fine subgrade. Since control has been found to be not significantly affected by the mean annual precipitation, its IRI curve for both precipitation levels overlap. As noted from Figure 3.2, all treatment levels lay below the control curve and, therefore, the application of the treatment slowed down the evolution of the roughness. Furthermore, the greater effectiveness of the PM treatments on wet areas noted from the interpretation of the model's parameters is reflected by the greater distance between the PM treatment curves and the control curve for the case of higher mean annual precipitation.

Figure 3.3 shows the predicted IRI curves corresponding to each PM treatment and control for two preexisting serviceability levels: the 15th (dashed lines) and 85th (solid lines) percentiles' initial IRI values. Since this variable affects only the sections with PM treatment, the control curves for both preexisting condition levels are parallel and shifted by the difference in initial IRI value. From the figure it is observed that the distance between the control curve and the PM treatments is greater for the case of lower initial IRI, which illustrates the greater effectiveness of the treatment when applied on smoother pavements.

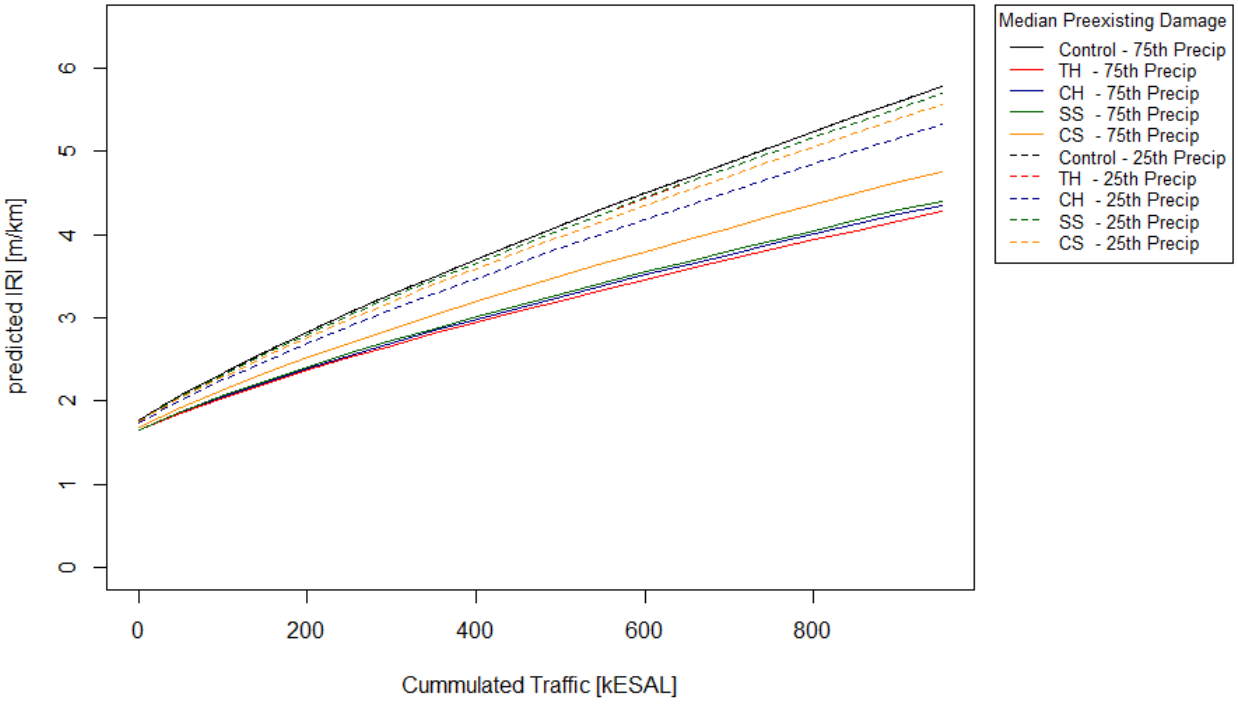

Figure 3.2: Comparison of predicted IRI curves for high and low annual precipitation

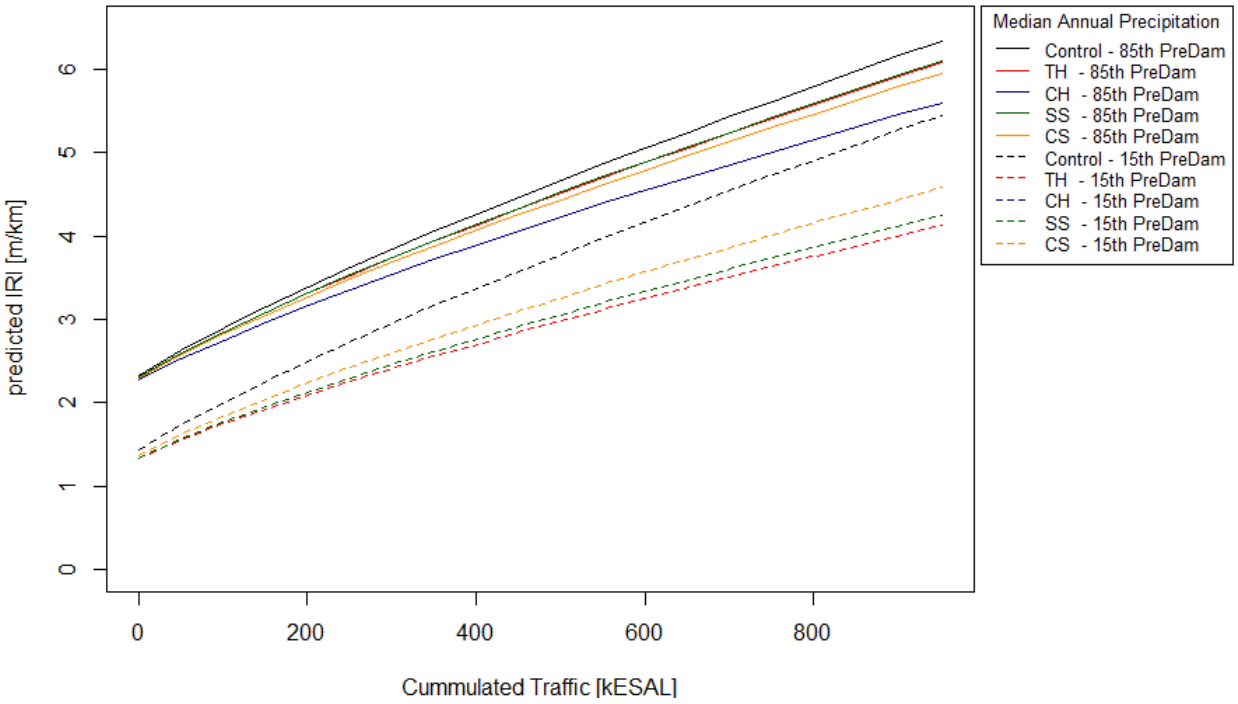

Figure 3.3: Comparison of predicted IRI curves for high and low preexisting damage values

3.8 Preliminary Summary and Conclusions

This section reports the preliminary analyses to study the effectiveness of four PM treatments applying a censored regression model-based approach using data collected for the LTPP SPS-3 experiment. The effectiveness of the PM treatments was evaluated as the difference in pavement DR relative to the non-treated sections, where DR was defined as the loss in serviceability (as measured by the IRI) per unit traffic. The DR model was specified as a function of the PM treatment type along with various experimental variables and followed a type 1 Tobit model structure in order to properly account for the significant portion of observations with censored DR.

The developed censored regression model allowed for estimating unbiased marginal effects of the different PM treatments accounting for multiple influence factors simultaneously. In addition, the study assessed the interaction between the treatments effectiveness and the different experimental factors in order to determine the optimal conditions for treating the pavement.

Following are the main observations and conclusions thus far:

- All four PM treatments presented slower serviceability loss relative to non-treated sections on an average base, for any given combination of cumulated traffic, environmental, and structural factors.
- TH and CH were more efficient than SS and CS in slowing down the evolution of pavement roughness relative to non-treated sections on an average base; however, the differences among treatments were not statistically significant.
- The estimated global marginal effects for the PM treatments ranged between -0.67E-03 m/km/kESAL (for SS) and -1.10E-03 m/km/kESAL (for TH). This marginal effect

results in 0.43 m/km (27 in/mile) to 0.26 m/km (16 in/mile) less IRI than if the section would not have been treated, after five years of median annual traffic and for an average pavement section.

- The effectiveness of the PM treatments was affected by the annual mean precipitation and by the pre-existing damage of the pavement, but not significantly affected by the section's average freezing index.
- All PM treatments but CS were significantly more effective when applied on sections with less preexisting damage. This observation reinforces the main purpose of applying PM, which is not to add structural capacity to the pavement but to delay its structural failure.
- All four PM treatments were significantly more effective when applied on sections with higher mean annual precipitation. This observation may be explained by the effect of the surface sealing provided by the PM treatments, which reduces the weakening of the pavement structure due to the presence of water.

Chapter 4. Progress to Date on Task Order No. 2: Quantification of Highway Pavement Surface Micro- and Macro-Texture

4.1 Background

According to the FHWA, in 2008, more than 19,000 people were killed in roadway departure crashes in the United States. Poor roadway conditions, especially wet pavement, have been identified as a major contributing factor in roadway departure crashes. It is estimated that about 70% of wet pavement crashes can be prevented or minimized by improving pavement friction, which is essential to achieve a good pavement performance. Pavement surfaces should be designed, constructed, and maintained in order to provide durable and adequate friction properties to the drivers.

Pavement surface texture is influenced by many factors, such as aggregate type and size, mixture gradation, and texture orientation, among others. The surface texture of an aggregate plays a leading role in providing high friction to a pavement surface. It is the property in charge of defining the skid resistance. Micro-texture and macro-texture are the two key pavement surface characteristics in the development of a good skid resistance. Micro-texture refers to the small-scale texture of the pavement aggregate component (which controls contact between the tire rubber and the pavement surface) while macro-texture refers to the large-scale texture of the pavement as a whole due to the aggregate particle arrangement (which controls the escape of water from under the tire and hence the loss of skid resistance with increased speed) (AASHTO, 1976).

The effect of the aggregate texture (micro-texture) and the effect of the texture of the compacted hot-mix asphalt (macro-texture) on the skid resistance of a highway surface are well recognized. However, there is a lack of fundamental understanding of the individual effect that each of these properties, micro and macro-texture, have on the final skid properties of the road. Most research studies in this regard have been based on theory, assumptions, and sound engineering judgement. The individual effects have not been quantified and their contribution to skid under different conditions of moisture, speed and highway conditions are not well understood. Recent developments in optics and computers allowed the collection of high definition 3-D images of the surface of the highway pavement. In particular, it is now possible to quantify micro-texture in the field in an effective and efficient manner. This can be done with the use of laser-based technology that allows measurements below 0.5 mm.

Locally, TTI has conducted a research using the Aggregate Imaging System (AIMS) to evaluate aggregate properties and to establish relationship with skid resistance. The AIMS combines hardware that captures real-time digital images of paving material samples, and software that analyzes shape, texture and ratio characteristics of aggregates. The AIMS is, however, an optical instrument whose resolutions does not allow the accurate quantification of micro-texture to the extent that laser does. Nevertheless, this project offers a unique opportunity to compare the findings of both studies and gain mutual benefit by evaluating the same sections and materials with both technologies and establishing meaningful comparisons.

4.2 Pavement Surface Properties

To achieve a good pavement performance, pavement surfaces should be designed, constructed, and maintained with durable and adequate friction and texture properties. Thus, in the

following sections, these parameters are described as well as the most common methods used to measure or test these relevant surface properties.

4.2.1 Texture

Pavement texture is the feature of the road surface that ultimately determines most tire/road interactions, including wet friction, noise, splash and spray, rolling resistance, and tire wear (NCHRP Synthesis 291, 2000). Pavement texture is the result of the deviations of the surface layer from a true planar surface. According to the Permanent International Association of Road Congresses (1987) and ASTM E 867 "Standard Definitions of Terms Relating to Traveled Surface Characteristics," these deviations can be classified in three different levels based on the wavelength (λ) and amplitude (A) of its components.

- **Micro-texture ($\lambda < 0.5\ mm$, $A = 1\ to\ 500\ \mu m$).**

  Micro-texture refers to the small-scale texture of the pavement aggregate component, which controls contact between the tire rubber and the pavement surface. The microscopic asperities of the aggregate particles are the responsible for the micro-texture.

- **Macro-texture ($0.5\ mm < \lambda < 50\ mm$, $A = 0.1\ to\ 20\ mm$).**

  Macro-texture refers to the large-scale texture of the pavement as a whole due to the aggregate particle arrangement, which controls the escape of water from under the tire and hence the loss of skid resistance with increased speed. The macro-texture provides drainage paths for the water entrapped between pavement surface and tire imprint (Huang, 2003).

  In asphalt pavements, the mixture properties (aggregate shape, size, and gradation), which define the type of mixture (dense, permeable friction course, stone matrix asphalt), control the macro-texture. In concrete pavements, the method of finishing (dragging, tinning, grooving; width, spacing, and direction of the texturing) controls the macro-texture.

- **Mega-texture ($50\ mm < \lambda < 500\ mm$, $A = 0.1\ to\ 50\ mm$).**

  This type of texture has wavelengths in the same order of size as the pavement-tire interface. It is largely defined by the distress, defects, or "waviness" on the pavement surface (NCHRP report 634, 2009).

A fourth level can also be considered: roughness/unevenness ($500\ mm < \lambda$). Roughness refers to the irregularities in the pavement surface that affect the ride quality, smoothness, and serviceability of a pavement. It affects the vehicle delay costs, fuel consumption and maintenance costs. The International Roughness Index (IRI), developed by the World Bank in 1980s, summarizes the longitudinal surface profile in the traveled wheelpath. It is commonly expressed in inches per mile (in./mi) or meters per kilometer (m/km). It can be computed from surface elevation data collected with a topographic survey or a mechanical profilometer. Many correlations have been developed between the IRI and the AASHTO Present Serviceability Index (PSI). Figure 4.1 illustrates these four levels.

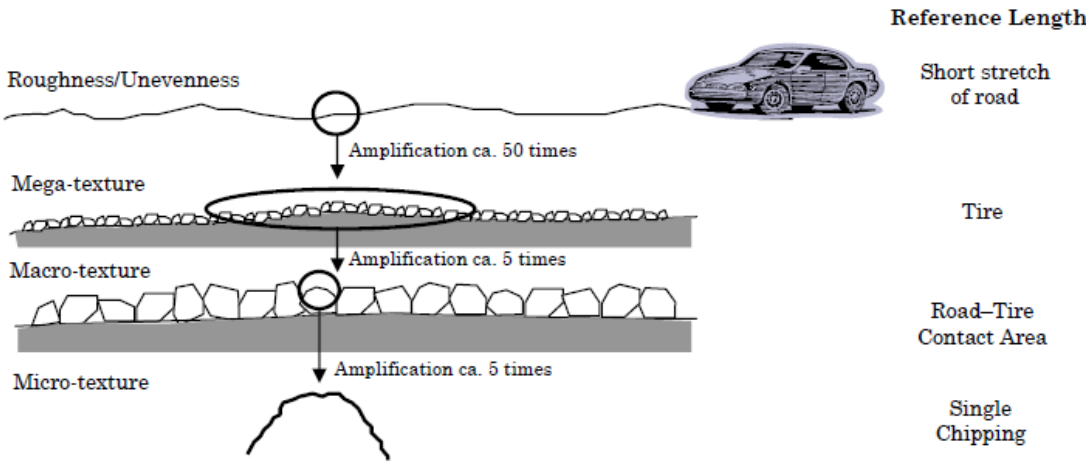

Figure 4.1: Simplified illustration of the various texture ranges that exist for a given pavement surface (Sandburg, 1998)

The division between macro and micro-texture is arbitrarily set. Nevertheless, these two parameters are the two key pavement surface characteristics to the development of a good skid resistance.

4.2.2 Friction

According to NCHRP 108 (2009), "pavement friction is the force that resists the relative motion between a vehicle tire and a pavement surface." As the tire rolls or slides over the pavement surface, the resistive force is generated. Thus, surface friction can be computed with Eq. 4.1.

$$F = \mu \cdot W$$

$$\boldsymbol{\mu = \frac{F}{W}} \tag{4.1}$$

where F is the tractive force applied to the tire at the tire-pavement contact, μ is the coefficient of friction, and W is the dynamic vertical load on the tire.

Skid resistance is the force developed when a tire that is prevented from rotating slides along the pavement surface. Skid resistance is commonly estimated using a friction measurement. If the coefficient of friction is multiplied by 100, the Skid Number (SN) can be estimated with Eq. 4.2:

$$SN = 100 \cdot \mu$$

$$SN = 100 \cdot \frac{F}{W} \tag{4.2}$$

Highway agencies should provide an adequate pavement surface friction (Figure 4.2) to prevent loss of control and give drivers the ability to maneuver their vehicles safely. The lower the friction between pavement and tire, the less control the driver has over the vehicle. It is important to understand that friction is not unidimensional; friction must be considered on the longitudinal and lateral directions. Friction is not only important for pavement design, but also for geometric

design of any roadway facility, as it is used to calculate the minimum horizontal and vertical curves and the minimum stopping sight distance, among other parameters.

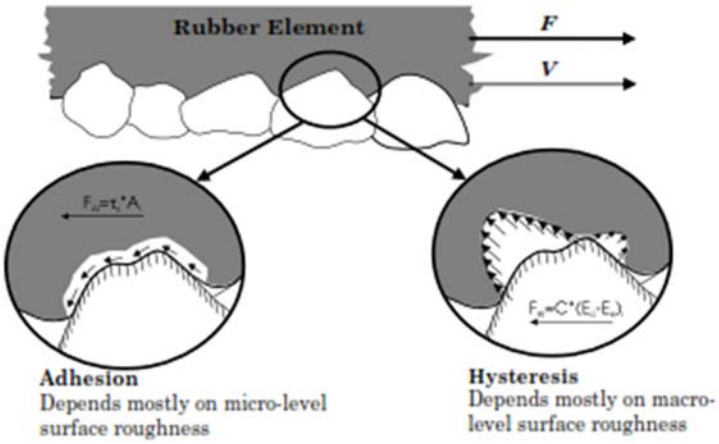

Figure 4.2: Key mechanism of pavement-tire friction (NCHRP 108, 2009).

The frictional force in pavements can be described by two major components: (1) adhesion and (2) hysteresis. Adhesion is the friction that results from the small-scale bonding/interlocking of the vehicle tire rubber and the pavement surface. It is a function of the interface shear strength and contact area. The hysteresis component of frictional forces results from the energy loss due enveloping of the tire around the texture. Because adhesion force is developed at the pavement–tire interface, it is most responsive to the micro-level asperities (micro-texture) of the aggregate particles. In contrast, the hysteresis force developed within the tire is most responsive to the macro-level asperities (macro-texture) formed in the pavement surface. As a result, adhesion governs the overall friction on smooth-textured and dry pavements, while hysteresis is the dominant component on wet and rough-textured pavements (NCHRP 108, 2009). In addition, two other components can be considered: (3) cohesion and (4) the viscous component of tire friction. The cohesion component represents the energy required to produce new surfaces. It is associated with the grooving of the tire and its abrasive wear. The viscous component refers to the shearing of a viscous layer between tire and road surface; it can occur only on wet roads (Ueckermann et al., 2014).

For pavements, the friction is affected by four major elements: driver, weather, vehicle, and roadway.

- *Driver*
  The skill of the driver affects the potential for loss of control or skidding. Skill level is related to a driver's level of experience, and can be affected by factors such as alcohol consumption. In highway geometric design, the PIJR (Perception, Identification, Judgement, and Reaction) time is essential to define the stopping sight distance.

- *Weather*
  The friction between tire and pavement is affected by the presence of water (i.e., rainfall or condensation). Wet conditions increase the potential for hydroplaning, during which the braking and steering effectiveness is reduced and the vehicle becomes uncontrollable. Thus, preventing the presence of excessive water on pavement is essential. Water's effect on friction is minimal at low speeds (less than 20 mph), but

increases exponentially at higher speeds. This effect is influenced by the tire design and conditions.

- *Vehicle*

Both a vehicle's design and the condition or structure of its braking system will affect its performance. For example, an anti-lock braking system (ABS) allows the wheels to maintain tractive contact with the road surface while braking, preventing the wheels from locking up (ceasing rotation) and creating uncontrolled skidding.

In addition, the vehicle operating parameters are critical to the interaction between the tire and the pavement surface. The higher the speed, the lower the coefficient of friction that can be developed. The tire tread design (type, pattern, and depth) and condition (i.e., older versus newer), as well as the tire pressure, have a critical impact on the friction, especially when water accumulates on the pavement surface. New, ribbed tires work better than smooth, fully worn tires. Under-inflated tires can considerably reduce friction at high speeds, and in wet conditions can prevent the flow of water through the treads. In contrast, tire over-inflation causes only small loss of pavement friction (Henry, 1983; Kulakowski et al., 1990).

A three-zone model (Moore, 1963) can be used to explain the contact conditions between the tire and pavement surface during rolling or skidding on a wet surface (Figure 4.3). In Zone A, the water completely separates the two surfaces and can be referred as the "squeeze-film" zone. Zone B, which is the "transition" zone, corresponds to the "mixed lubrication" zone, where the tire thread elements, having penetrated the squeeze-film, commence to cover over the major asperities. Zone C is the actual contact or traction zone where dry contact can be established. The zone lengths depend on vehicle speed and the amount of water that has to be expelled from the interface. Due partly to the lubricant function and partly the sliding velocity used in skid resistance measurements, adhesion is largely inhibited and hysteric friction is the dominant mechanism (Ueckermann et al., 2014).

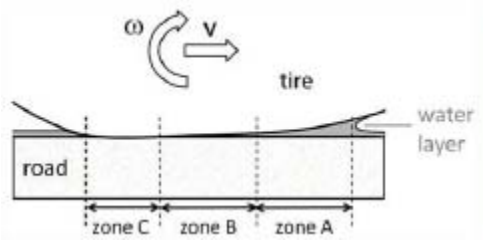

Figure 4.3: Three-zone model (Moore, 1963).

- *Roadway*

The properties of the pavement surface materials (aggregate and mixture characteristics) help to define surface friction and texture, as well as pavement conditions over time. The capacity of the aggregates and the mix to resist polishing and abrasion/wear under traffic is directly related to the pavement's ability to retain the good condition of its surface properties. Pavement friction is a time-dependent parameter. During the first years after construction, crashes are more common due to the low pavement friction. Once the roadway surface is worn away and the aggregates

are exposed by the passage of vehicles, the friction levels are increased. Then, ultimately, friction will again decrease as the pavement further ages.

Furthermore, friction qualities are reduced by the smoothness of polished aggregates, bleeding, and rutting, as well as inadequate cross slope, which increases the thickness of the water layer, as the time required for the water to drain from the pavement surface also increases (creating the potential for hydroplaning).

4.3 Skid Resistance and the Effect of Micro- and Macro-Texture

The skid resistance of a pavement heavily relies on its micro- and macro-texture. In micro-texture, a weak bond between the grains of an aggregate causes the aggregate to wear, but provides a continually renewed non-polished surface. On the other hand, if the grains are bonded tightly, the grains will be polished by the continuous traffic. Therefore, in order to have good skid resistance, aggregates should contain two minerals of different hardness in order for the aggregate to be polished unevenly, maintaining a rough surface.

In macro-texture, the angularity of the aggregates has a major effect on the skid resistance of a pavement. Angular aggregates are more skid resistant; however, constant traffic crushes them into flat and elongated particles, diminishing the skid resistance. In asphalt pavements, large aggregates increase skid resistance, but require high-quality coarse aggregates. In a concrete pavement, sand-size aggregates have a greater influence due to the cement mortar on the surface, which also calls for high-quality fine aggregates. When it comes to large aggregates in Portland cement concrete (PCC), only the exposed aggregate affects the skid. However, in both pavement types, the size of the largest aggregates (exposed aggregates in PCC) provides the dominant macro-texture wavelength if closely and evenly spaced.

The macro-texture can also be improved in a concrete pavement through the use of texturing existing pavement. Concrete can be textured from 0.019 in. to 0.045 in. in order to improve the skid resistance. Examples of texturing include tining, grooving, grinding, and turf dragging. Asphalt can also be textured, but on hot days the asphalt binder can fill in the grooves. Asphalt binder also affects the micro- and macro-texture because bleeding of the binder will reduce the skid resistance.

A tough binder is ideal to prevent skid. The gradation of an asphalt mixture or a PCC with exposed aggregate can also have a major effect on the skid resistance. A porous asphalt mixture allows for more air voids, which leads to better pavement drainage and increased friction. For both asphalt and concrete pavements, there are many ways to alter the macro-texture by adjusting the aggregate types, the mix gradation, air content of asphalt mixture, and texture orientation. However, the micro-texture is limited to alteration only through the selection of the coarse aggregate type for asphalt and exposed-aggregate PCC, and through selection of the fine aggregate type for concrete. Thus, adjusting skid resistance a completed pavement through macro-texture is more feasible.

4.4 Aggregate Properties and Selection

4.4.1 Properties

Design of hot-mix asphalt (HMA) pavements mainly includes the aggregate and bituminous binder. Typically, a mixture is composed of approximately 95% aggregate and 5% bituminous binder by weight depending on the requirements for the application and availability of

materials. Given that the amount of aggregate that is used in a single asphalt mixture is so high, the engineer must carefully consider the various physical, chemical, and mechanical properties of the aggregate for the specific application. In other words, depending on the intended use and the desired performance, some properties will be more significant than others.

Some of the key characteristics in selecting the proper aggregate for a specific application include shape, angularity, and texture. These can significantly influence the performance of the pavement; consequently, aggregates with certain properties are preferred and specified for these mixtures. Sufficient levels of particle strength and stiffness are essential to provide the best interlocking between the different particles, creating a better and stronger pavement.

Specification can describe aggregates in many different shapes and sizes. Most standards describe the shape of an aggregate particle as cubic, blade, disk, or rod shaped. Typically, aggregates with higher crushed faces (cubic) are preferred over rounded, smooth particles for asphalt mixtures, as they promote interlocking of aggregate particles—ultimately resulting in a stronger, more stable pavement. Angular particles provide more shear strength and tend to dilate more instead of fracturing. Rounded, smooth particles tend to slip past each other (resulting in lower shear strength), thus providing less strength than an angular particle. Most asphalt mixture specifications limit the amount of aggregate particles with rounded, smooth texture used, as these mixtures are designed to provide enough stability and strength to the matrix.

Particle shape, strength, and stiffness are directly related to the particle grading and the surface texture of the material. If the material presents a single size aggregate and a smooth texture, it would be very difficult to achieve a good interlocking. The shape of aggregates can also highly influence the amount of bituminous binder that is used in a pavement mixture. Particle grading specifies the types of sizes and weight fraction for each aggregate. Larger, single-sized, and rounded aggregates produce more voids (empty space) in the pavement matrix and require more binder material to completely bind the aggregates together.

It is important to have a good dense mass of material in order to reach rigidity. This type of gradation allows different aggregate types and sizes—from coarse to fine—to occupy most of the pavement volume. In addition, in bituminous mixtures, the grading will be responsible for defining many of the pavement's characteristics: permeability, noise, strength, and surface texture, among others. In any pavement design, the type of gradation achievable will depend upon the materials that will be available near the construction/production area. Otherwise, the most technically compliant solution could be prohibitively expensive. In addition, dense graded mixtures require less binder and consequently are more economical.

As discussed earlier, the surface texture of an aggregate plays a leading role in providing high friction to a mixture. It is the property that defines the skid resistance. In addition, a rough texture will help to generate a good bond between the binder and the aggregate. In contrast, smooth aggregates could lead to segregation in the mixture.

Another important property of an aggregate is its pore structure. It is essential to know if the aggregates present many pores and what level of permeability the structure will provide. In asphalt mixtures an impermeable (isolated and enclosed cavities) and low-volume pore structure is preferred, as it will not absorb more binder and water than is ideal—thus minimizing the freeze-thaw effect and absorption.

Particle shape and grading, texture, and the pore structure are linked to the voids in the aggregate mixture, which minimize the binder requirements and maximize the economy of the construction.

Furthermore, aggregate presents chemical properties that should be also considered in an asphalt mixture design. Coating and surface charges are directly related to the adhesion between the aggregates and bitumen. A good connection between these entities should be provided in order to improve the performance of the asphalt mixtures. In addition, surface charge plays a key role in the emulsions design.

4.4.2 Selection of Aggregates

In order to provide the adequate aggregates for an HMA, the Superpave system specifies three different tests to classify shape and angularity of the aggregate particles. However, this system does not provide any test to measure the surface texture.

The tests described below do not represent the more efficient procedures to classify and estimate this characteristics of an aggregate. Newer methods using imaging techniques have been developed in the last years.

Aggregate shape: "Standard test for flat particles, elongated particles, or flat and elongated particles in coarse aggregates" (ASTM D 4791)

This test specifies a maximum percentage by weight of coarse aggregates that have a maximum to minimum dimension-ratio greater than five (5:1 ratio). Elongated particles are undesirable because they have a tendency to break during construction and under traffic. The test procedure is performed on coarse aggregate larger than 9.5 millimeters. The procedure uses a proportional caliper device to measure the dimensional ratio of a representative sample of aggregate particles (Superpave, 2002).

Coarse aggregate angularity: "Standard test method for determining the percentage of particles in coarse aggregate" (ASTM D 5821)

The test specifies a minimum percentage by weight of aggregates larger than 4.75 mm with one or more and two or more fractured faces. The minimum values depend upon the traffic level and layer in the pavement structure. A face will be considered a 'fractured face' only if it has a projected area at least as large as one quarter of the maximum projected area (maximum cross-sectional area) of the particle and the face has sharp and well defined edges; this excludes small nicks (Superpave, 2002).

Fine aggregate angularity: "Uncompacted void content method A" (AASHTO T 304)

This test specifies the minimum percentage of air voids in loosely compacted aggregates smaller than 2.36 mm. Higher void contents correspond to higher fractured faces. By determining the weight of fine aggregate (W) in the filled cylinder of known volume (V), void content can be calculated as the difference between the cylinder volume and fine aggregate volume collected in the cylinder. The fine aggregate bulk specific gravity (G_{sb}) is used to compute fine aggregate volume (Superpave, 2002).

4.5 State of the Art

An extensive literature search and review was conducted to determine the state of the practice and the state of the art in terms of field measurement of micro- and macro-texture. The literature review also focused on identifying theory and models that relate micro- and macro-

texture measurements to skid resistance at various speeds and under different conditions. In addition, the properties and measurements performed by the AIMS were evaluated and compared with the Laser Texture Scanner (LTS).

4.5.1 Aggregate Imaging Measurement System (AIMS)

The AIMS (shown in Figure 4.4) uses camera, lighting, and microscope technology to analyze the particle geometry of coarse and fine aggregates through three independent properties: form, angularity (or roundness), and surface texture. Coarse aggregates sizes passing the 37.5 mm sieve and retained on the 4.75 mm (No. 4) sieve can be evaluated, as well as fine aggregate passing the 4.75 mm (No. 4) sieve and retained on the 0.075 mm (No. 200) sieve.

Figure 4.4: AIMS components (Alrousand, 2004).

The classification methodology can be used for the evaluation of the effects of different processes (such as crushing techniques and blending) on aggregate shape distribution, and for the development of aggregate specifications based on the distribution of shape characteristics (Masad et al., 2005). It also has the capability to characterize the surface of asphalt cores for micro- and macro-texture parameters.

In order to perform this analysis, the device captures images at different resolutions with a camera, and uses different arrangements of lighting to provide uniform illumination. In this way, different image analysis techniques can provide accurate results.

AIMS uses a 3-d analysis of coarse particles, which allows distinguishing between flat, elongated, or flat and elongated particles. On the other hand, a 2-d analysis is used for fine particles. In addition, by using the fundamental gradient and wavelet methods, it quantifies angularity and the surface texture respectively (Masad et al., 2005). Pavement micro-texture can be described by the surface texture of the aggregates.

If the particles analyzed are coarse, black and white images are used to quantify form and angularity, while gray images are used for texture. These aggregates are analyzed individually by placing them in a backlighting sample tray, which has marked grid. This task is labor intensive,

but once it is done, the device analyzes automatically all the particles. On the other hand, black and white images are used to evaluate all these properties in fine particles. In this case, the particles are randomly placed on the aggregate tray with the backlight turned on. AIMS angularity characterizes the particle edge sharpness characteristics on a scale of 0-10000. The principles involved in analyzing all the parameters are discussed below.

Radius Method (Angularity)

In the radius method, the angularity index is measured as the difference between the particle radius in a certain direction to that of an equivalent ellipse; see Eq. 4.3.

$$Angularity\ Index = \sum_{\theta=0}^{355} \frac{|R_\theta - R_{EE\theta}|}{R_{EE\theta}} \tag{4.3}$$

where R_θ is the radius of the particle at an angle of θ, and $R_{EE\theta}$ is the radius of the equivalent ellipse at an angle of θ (Masad et al., 2005).

Gradient Method (Angularity)

The rationale behind this method is that at sharp corners of the image, the direction of the gradient vector changes rapidly—but changes slowly along the outline of rounded particles (Bathina, 2005). Thus, the angularity analysis is performed by estimating the angle of orientation (θ) of the edge points and the magnitude of difference of these values ($\Delta\theta$). If these differences are significant, a sharp angularity is described. A small value corresponds to a rounded edge.

The angularity index is calculated by the sum of angularity values for all the boundary points accumulated around the edge of the aggregate particle. For the ***gradient method***, angularity is mathematically represented as Eq. 4.4:

$$Angularity\ Index\ = \sum_{i=1}^{N-3} |\theta_i - \theta_{i+3}| \tag{4.4}$$

where *N* is the total number of points on the edge of the particle with the subscript i denoting the i^{th} point on the edge of the particle (Masad et al., 2003).

Sphericity (Form Analysis)

The form is quantified in three dimensions, which estimate the sphericity of the particle, as in Eq 4.5.

$$Sphericity = \sqrt[3]{\frac{d_s \cdot d_l}{{d_L}^2}} \tag{4.5}$$

where d_s is the shortest dimension of the particle, d_l is the intermediate dimension, and d_L is the longest dimension.

The two major and minor axes are analyzed from the black and white images (Eigen vector analysis) while the depth of the particle is measured by auto focusing the microscope (Fletcher et al., 2003).

Form Index (Form Analysis)

The form index uses incremental change in the particle radius and is expressed by Eq. 4.6:

$$Form\ Index\ = \sum_{\theta=0}^{\theta=360-\Delta\theta} \frac{|R_{\theta+\Delta\theta} - R_{\theta}|}{R_{\theta}} \tag{4.6}$$

where R_θ is the radius of the particle at an angle of θ; and $\Delta\theta$ is the incremental difference in the angle (Bathina, 2005).

Texture Analysis

To describe the texture content at a given resolution or decomposition level, a parameter called the wavelet texture index is defined. The texture index at any given decomposition level is the arithmetic mean of the squared values of the detail coefficients at that level. The texture information lies in the detail coefficients LH, HL, and HH. The LH coefficients pick up the high frequency content in the vertical direction, the HL coefficients pick up the high frequency content in the horizontal direction, and the HH coefficients pick up the high frequency content in the diagonal direction. The texture contents in all directions are given equal weight and the texture index is computed as the simple sum of squares of the detail coefficients at that particular resolution. The texture index is given by Eq 4.7 (Masad et al., 2005). The AIMS characterizes surface texture on a scale of 0–1000.

$$Texture\ Index_n\ = \frac{1}{3 \cdot N} \sum_{i=1}^{3} \sum_{j=1}^{N} \left[D_{i\,j}(x, y) \right]^2 \tag{4.7}$$

where n is the decomposition level; N is the total number of coefficients in a detailed image of texture; i takes values 1, 2, or 3 for the three detailed images of texture; j is the wavelet coefficient index; and (x, y) is the location of the coefficients in the transformed domain (Masad 2005).

Figure 4.5 diagrams the AIMS process.

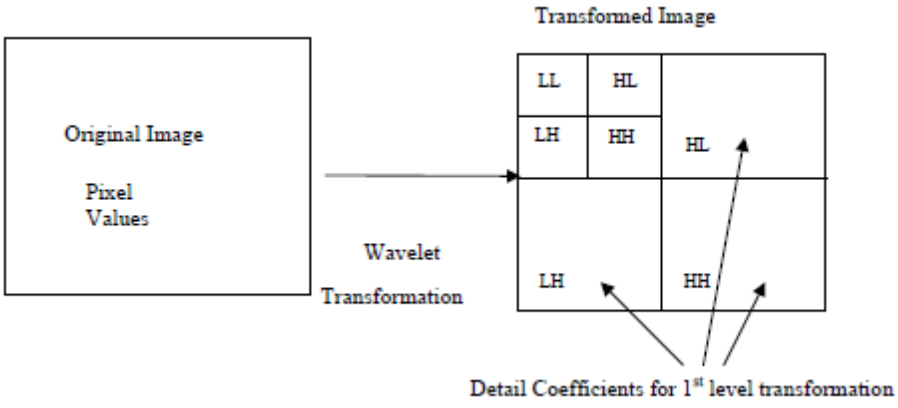

Figure 4.5: AIMS process (Masad, 2005).

Advantages

- Automated classification of aggregates.
- Very accurate and fast method for quantifying and evaluating aggregate form, angularity, and texture.
- More efficient than the test specified by the Superpave system.
- Pavement micro-texture is described by the texture of the aggregate.

Disadvantages

- The device is not portable. Therefore, it is only applicable in the laboratory.
- It has its own system of aggregate form, angularity, and texture classification.
- It is only applicable for aggregates.
- The equipment is expensive.

4.5.2 Laser Texture Scanner (LTS)

The LTS (Figure 4.6) is a lightweight and portable equipment produced by Ames Engineering, which "is designed to scan and precisely measure the texture content of any type of surface" (Ames, 2010). This laser scanner is designed to measure and describe the two decades of the macro-texture (wavelengths between 50 mm to 0.5 mm) and the first decade of the micro-texture (wavelengths between 0.5 mm to 0.05 mm). In fact, this device can even measure wavelengths up to 0.03 mm.

Figure 4.6: LTS (top) and circular track meter (bottom).

The LTS uses a laser sensor to scan the surface coordinates of parallel straight lines with a high sampling rate of one point every approximately 0.015 mm (Serigos et al., 2014). It has a maximum scan length of 4.1 in. (104.14 mm), and a maximum scan width of 3.0 in. (76.20 mm), which allows a maximum of 1200 line scans (spacing of 0.064 mm between lines). The scanner will perform the selected amount of lines scans of equal spacing over the width. The LTS is placed on the surface through three point contact feet.

Once a scan is concluded, the LTS immediately calculates five indexes. The average results for the entire scan are displayed on a sunlight-readable LCD display.

- *Mean Profile Depth (MPD)*
  The device has the option of applying a 2.5mm filter to the data before calculating the MPD. This filter removes wavelengths smaller than 2.5mm. The ASTM E 1845 specification for calculating MPD requires that this filter be applied. The LTS maximum scan length complies with the ASTM requirements for the MPD calculation which requires a line scan length of 100 mm.
- *Estimated Texture Depth (ETD)*
  The ETD (ASTM E 1845) is an estimation based on MPD that correlates well to volumetric testing techniques (sand patch test).
- *Texture Profile Index (TPI)*
  The TPI calculates the least-squares-fit line for the scan data, and then looks for deviations above and below that line. When the texture profile goes up and crosses the line and then comes down again later and crosses the line, the highest peak in that event is called a positive scallop height. When the texture profile goes down and passes through the line and then later goes positive and crosses the line, the lowest point in that event is called a negative scallop height. The index is calculated by summing up the absolute value of all the positive and negative scallops in the entire scan. The sum value is than divided by the total number of scan lines. The result of this calculation is the average height of all scallops in the scan line.
- *Root Mean Square (RMS)*
  The RMS calculation is done by first removing the least-squares-fit line from each scan line, and then calculating the RMS of the resulting data.
- *Variance (VAR)*
  The Variance calculation can be done on either the elevation profile (EEV for English Elevation Variance measured in inches, and MEV for Metric Elevation Variance measured in mm), or the slope profile. The Variance Index calculation allows the user to filter the scan line data into three separate band pass filtered wavebands and calculate the elevation or slope variance of each data set. The exponent-weighting field is used to make the LCD display more usable for small numbers.

By default the first waveband is from 50 mm to 5 mm, which is indicated by an “L=” for the long macro wavelengths. The next band is from 5 mm to .5 mm, which is indicated with an “S=” for short macro wavelengths. The third waveband is from .5 mm to .04 mm and is indicated with an “M=” for micro wavelengths.

The data collected can be downloaded from the device through an Ethernet connection. Three different files are created. The results of the selected indices for each scan line are displayed

in an HTML file and a CSV file (each of which are named 'Results'). The 'Data' CSV file compiles all the data points collected per line by the scanner. This file provides all the needed information to process and analyze the data collected in other types of software like Microsoft Excel or MatLab. Ames Engineering provides its own software to analyze the collected files and display a navigable 3-D graph of the scan.

The LTS has the ability to control the intensity of the laser spot. Half power setting works best when scanning bright white surfaces with no sunlight striking the surface of the scan area. Direct sunlight will cause spikes to occur in the data and will elevate the measurements being made. On the other hand, the full power setting works best for very dark surfaces, or for scanning outside in the sunlight. If full power is used on very white surfaces, small spikes may occur in the scan data. Spikes occur when the laser cannot see the bottom of a deep crack because of the angle of the returning light to the detector. The sensor increases the intensity of the laser light causing the crack in the scanned surface to glow, which confuses the detector and creates a spike in the data (LTS User Manual, 2010).

Unlike AIMS, the LTS is portable and is powered using rechargeable batteries and a built-in charging system. Thus, it is the perfect device to collect data in the field. A GPS receiver option allows tracking of the GPS location of each texture measurement taken out in the field.

Advantages

- It is a portable device and can collect GPS data.
- It provides good repeatability and reproducibility when a few line scans are selected.
- Good for quality control and quality assessment of texture.

Disadvantages

- It requires traffic control and lane closure.
- Depending upon the precision required, it can be time consuming. In any case, several measurements are required if a network evaluation is performed.
- When triangulation sensors are unable to see the laser dot on the surface with its camera, it will hold the last good elevation value it was able to read. It is estimated that the number of points collected with the same elevation value is between the 25 and 35% of the points collected, which reduces the device precision.

4.5.3 Studies by the Texas A&M Transportation Institute (TxDOT Project 0-5627)

The objectives of the research performed by TTI (Masad et al., 2010) were to:

- Study the influence of aggregate properties and mix types on asphalt pavement skid resistance.
- Develop a database of the annual field skid resistance data.
- Develop a system for predicting asphalt pavement skid resistance during its service life.

In order to achieve these goals, gradation, aggregate texture, and mixture friction were estimated as a function of the number of polishing cycles in the lab. Five different aggregate

sources and a blend of two Texas sources were polished using the Micro-Deval test (ASTM D6928) for two different time durations: 105 and 180 minutes. The texture of polished aggregates was measured using AIMS after those polishing cycles. In addition, large asphalt slabs were compacted in the laboratory using three mixtures commonly used in Texas: Type C, Type D (both of which are dense-graded mixes), and PFC (permeable friction course). These slabs were polished at three locations by the three-wheel polishing device originally developed at the National Center for Asphalt Technology. By using the dynamic friction tester (DFT) (ASTM E 1911) and the circular track meter (CTM) (ASTM E 2157), friction and texture measurements were performed before any polishing and after predefined polishing cycles: 100,000, 5,000 and 200,000 cycles respectively.

- Aggregate gradation (Weibull distribution function) (Eq. 4.8)

$$F(x,k,\lambda) = 1 - e^{(-x/\lambda)\cdot k} \tag{4.8}$$

  where x is aggregate size (mm), and κ and λ are known as the shape and scale parameters.

- Aggregate texture (Eq. 4.9)

$$Texture\ (T) = a_{agg} + b_{agg} \cdot e^{-c_{agg}\cdot t} \tag{4.9}$$

- Mixture friction as a function of number of polishing cycles (Eq. 4.10)

$$IFI(N) = a_{mix} + b_{mix} \cdot e^{-c_{mix}\cdot N} \tag{4.10}$$

  where a, $a+b$, and c are the terminal, initial, and rate of change in the texture or IFI (International Friction Index), t is the polishing time (min), and N is the number of increments of 1000 polishing cycles.

The model proposed in this study can predict the friction of a mix based on gradation and the polishing resistance of aggregates, as well as to help classification or selection of aggregates and mixes according to its frictional properties.

In addition, an extensive data collection and analysis was conducted to create a database of sections with different friction characteristic, mixes, and aggregates that could be correlated with the laboratory measurements (Figure 4.7 and Figure 4.8). "These data and measurements were used to carry out comprehensive statistical analyses of the influence of aggregate properties and mixture design on skid resistance value and its variability" (Masad et al., 2010).

Data of skid resistance measurements using the skid trailer were collected for many field sections (65 roads, including 1527 PMIS sections) with known construction history. Four surface types (surface treatment Grade 3, surface treatment Grade 4, PFC, and Type C) were included in the analysis. As long as gradation remained the same, regardless of asphalt type, the surface treatment was assumed to be the same. To compare different road categories in service years, it was introduced a new parameter, show in Eq. 4.11: Traffic Multiplication Factor (TMF).

$$TMF = \frac{AADT \cdot Years\ in\ Service \cdot 365}{1000} \quad (4.11)$$

It was observed that the surface treatments had a very high variability in their measured SN using skid trailer because this value is not just a function of aggregate shape characteristics and gradation, but other factors such as overall macro-texture of pavement surface. Also documented was a great deal of interaction between the aggregate performance, mix type in which aggregate is used, and traffic level. The results showed that the surface aggregate classification system does not always yield consistent skid resistance.

The same equation form used to describe aggregate polishing rate was considered a good predictor to describe SN vs TMF values in the field, and SN vs polishing cycles in the laboratory. It was observed that measured SN decreased as TMF increased, and had less variation at higher TMF levels. This effect could be attributed to mixtures reaching close to terminal skid condition, which is associated with aggregates approaching their equilibrium (or terminal) state of texture after a high number of polishing or loading cycles.

District	County	Highway	Des.	Mix Design	TRM	Dir.
Abilene	Nolan	IH20	L	CRM	247+0.1	WB
	Taylor	IH20	L	PFC	272+0.1	WB
				Superpave 1/2"	280+0.8	WB
				PFC	284-0.55	WB
		US83	L	PFC	328-0.30	NB
Atlanta	Harrison	IH20	R	SMA-C	634+320'	EB
Austin	Bastrop	US290	K	PFC	628+0.53	EB
	Travis	SH71	L	Type C	582-0.61	WB
Beaumont	Hardin	FM421	K	Type C	747+0.7	EB
		US69	K	SMA-D	489+0.1	SB
	Jefferson	SH73	L	PFC	772+0.1	WB
		US69	L	PFC	538-0.05	NB
	Tyler	SH146	K	Type C	422+0.7	NB
Brownwood	Brown	FM2376	K	Type D	460+1.6	NB
		FM2524	K	Type D	340+ 0.4	SB
		FM3064	K	Type D	458+0.9	WB
		SH153	K	Type D	372+0.7	WB
		US67	K	Type D	570+0.4	WB
	Eastland	IH20	L	Type D	362+0.6	WB
		SH36	K	Type C	346+1.6	WB
	McCullough	US87	R	Type D	458+0.2	SB
Bryan	Limestone	US84	K	Type C	736+150'	EB
Corpus Christi	Nueces	IH37	R	PFC	15+0.73	NB
	San Patricio	IH37	R	PFC	17+0.64	NB
Fort Worth	Johnson	IH35	WL	Type D	29-100'	SB
Houston	Brazoria	SH288	R	PFC	496+1.35	SB
	Conroe	IH45	L	PFC	93+0.1	SB
	Fort Bend	SH6	K	PFC	682+0.75	SB
	Waller	SH6	L	PFC	628+1	NB
Lubbock	Crosby	US-62	L	CMHB-C	352+1.7	WB
	Floyd	US-62	R	CMHB-C	386+0.1	EB
	Garza	SH207	K	CMHB-F	254+1.7	SB
		US84	L	CMHB-C	352+1.7	NB
	Lynn	FM1317	K	CMHB-F	296 +80'	EB
		US380	K	CMHB-C	320+1.7	EB
		US87	L	CMHB-C	306+1-400'	NB
	Terry	US62	L	Novachip	296+0.5+100'	WB
Odessa	Ector	IH20	R	CMHB-F	117+0.7	EB
	Midland	IH20	R	PFC	147+0.5+400'	EB

Figure 4.7: Measured field sections (Masad et al., 2010).

District	County	Highway	Des.	Mix Design	TRM	Dir.
Paris	Hopkins	IH30	L	PFC	134-.035	WB
		SH154	K	Type D	674-0.74	NB
San Antonio	Bexar	IH35	R	PFC	168+0.8	NB
		SH16	R	Type C	614	SB
		US90	R	Type C	560+1.75	EB
	Wilson	US181	R	Novachip	518	SB
Tyler	Anderson	US287	K	Type D	604+0.1	NB
	Greg	IH20	L	Type D	580+0.7	WB
				Type C	591-200'	WB
	Smith	IH20	L	Type C	550-500'	WB
				Type C	557-500'	WB
	Van Zandt	IH20	L	Type C	518-200'	WB
Waco	Hill	IH35	L	SMA-D	358-200'	SB
	McLennan	SH6	L	PFC	502-0.1	WB
Wichita Falls	Clay	US287	K	PFC	532+0.5	NB
		US287	L	PFC	368 + 1.8	WB
	Wichita	SH240	L	PFC	470-0.85	NB
		SL473	K	PFC	192-0.35	SB
Yoakum	Gonzales	IH10	L	PFC	636+0.2	WB
	Victoria	US59	L	Type C	632+60'	NB
		US59	R	PFC	632+0.5	SB
				PFC	634+120'	SB
	Wharton	US59	L	Type C	562-550'	NB
		US59	R	PFC	560+1+260'	SB
	Austin	SH36	K	Type D	612+1.5+200'	SB

Figure 4.8: Measured field sections (Masad et al., 2010).

Furthermore, CTM and DFT measurements were conducted on 64 pavement sections with a record of skid measurements for several years, construction history, and diverse range of weather and traffic conditions. The pavement age of these sections was between 2 and 11 years. Measurements were completed on the left wheel path of the outer lane (four locations per section) to correlate with the SN measured by the skid trailer, and on the shoulder (two locations per section) to obtain the initial skid measurements of the travel lane (shoulders are subjected to little or no traffic). These sections did not include any surface treatments. The TMF on the test section was calculated considering that all the vehicles types had the same polishing effect on the road surface, a 50/50% distribution, and traffic lane distribution factors. See Eq. 4.12–4.14.

$$IFI = 0.081 + 0.732 \cdot DFT_{20} \cdot e^{-40/S_p} \tag{4.12}$$

$$IFI = 0.045 + 0.925 \cdot 0.01 \cdot SN(50) \cdot e^{20/S_p} \tag{4.13}$$

$$S_p = 14.2 + 89.7 \cdot MPD \tag{4.14}$$

where DFT_{20} is the dynamic friction at 20 kph. Figure 4.9 provides the layout used in the Masad et al. study, while Figure 4.10 relates the MPD values for various mix types.

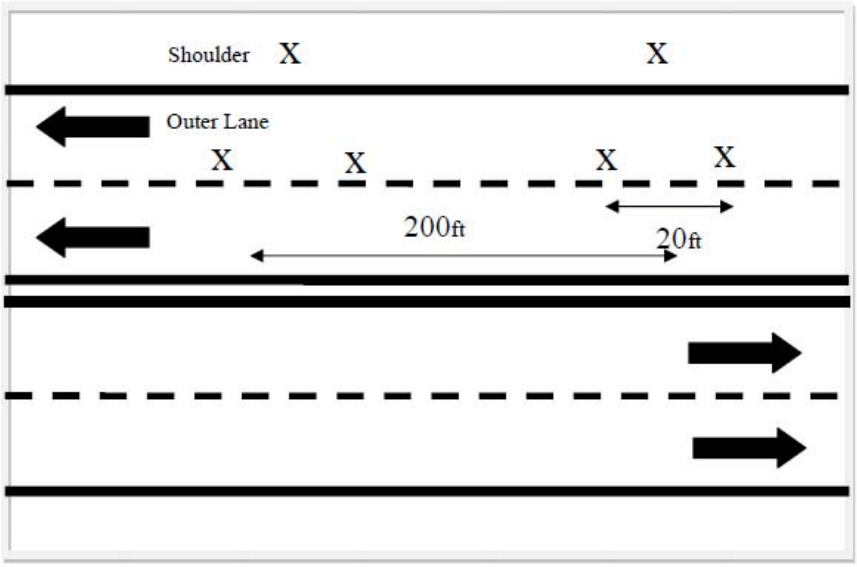

Figure 4.9: Layout of the measurement section (Masad et al., 2010).

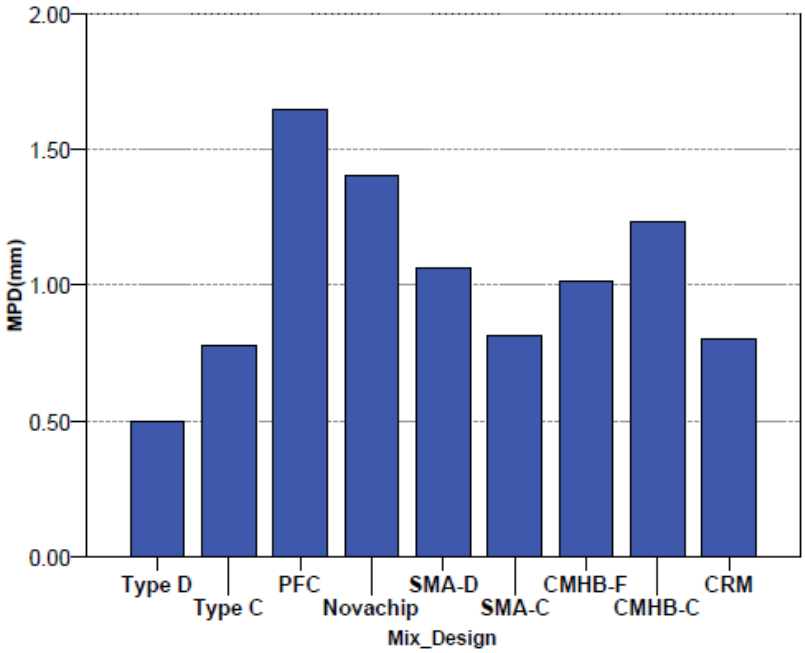

Figure 4.10: Measured MPD values for different mix types (Masad et al., 2010).

PFC mixes, because of their porous composition, presented a higher MPD, which allows water to drain faster. Among the dense mixes, Type D had the lowest MPD values, as the mix had more fine particles than Type C. The results indicated that there was no direct relationship between MPD and measured SN (Figure 4.11). Dynamic friction measured by DFT described the micro-texture, whose initial level depends on aggregate type. In addition, there was a fair correlation between friction (DF20) and measured SN for all mixes.

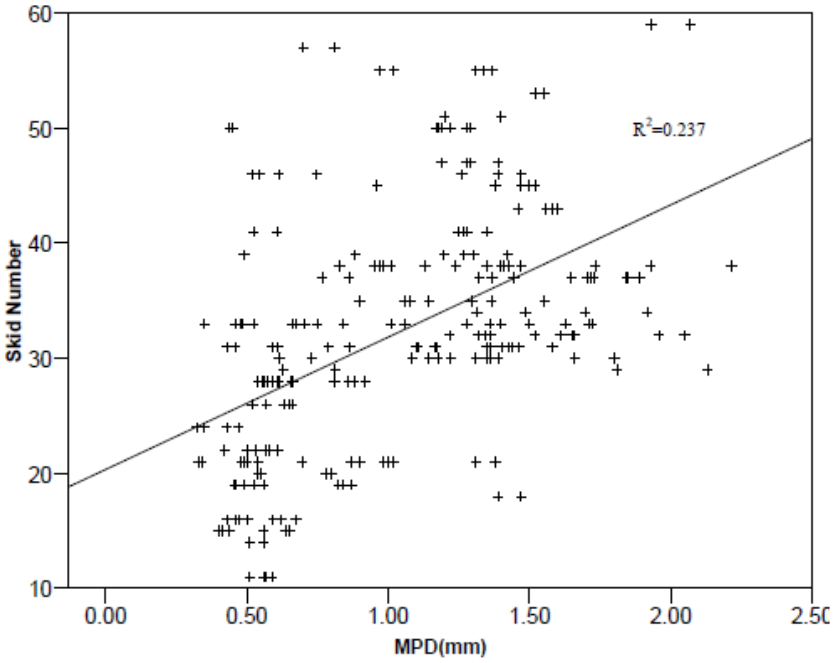

Figure 4.11: MPD vs measured SN (Masad et al., 2010).

The influence of certain aggregate parameters (texture) on mixture skid resistance also depends on the type of mixture design. Thus, a method and software were developed to predict the SN of asphalt pavements as a function of traffic based on aggregate characteristics and mixture design gradation. This method requires inputs that describe aggregate resistance to polishing, mixture gradation, and traffic.

This system consists of the following steps:

- Measure aggregate texture using AIMS before Micro-Deval (BMD).
- Measure aggregate texture using AIMS after Micro-Deval (AMD).
- Calculate $a_{agg} + b_{agg}$.
- Calculate a_{agg}.
- Calculate texture loss (TL) (Eq. 4.15).

$$TL = \frac{BMD - AMD}{AMD} \tag{4.15}$$

- Calculate aggregate roughness index (ARI) (Eq. 4.16).

$$ARI = \frac{AMD/BMD}{\sqrt{1-(AMD/BMD)^2}} \tag{4.16}$$

- Calculate c_{agg}.

- Determine the gradation parameters (λ and κ) by fitting the cumulative Weibull function to the gradation curve. Note: A table with values for TxDOT mix designs is provided.
- Calculate a_{mix}.
- Calculate $a_{mix} + b_{mix}$.
- Calculate c_{mix}.
- Calculate MPD.
- Calculate SP.
- Calculate International Friction Index (IFI) as a function of the polishing cycles (N)
- Calculate TMF in terms of N.
    - The relationship between N and TMF is not only a function of traffic but also a function of mixture polishing characteristics.
- Calculate SN.
- Predict the SN value given the IFI.
    - In order to obtain the relationship between measured skid resistance by skid trailer and DFT/CTM combination, the sensitivity analysis was conducted using several aggregate types and mixture designs.

4.5.4 Studies by The University of Texas at Austin

This study performed by UT Austin (Serigos et al., 2014) explored "different methods to characterize the micro-texture of pavement surfaces with the main objective of quantifying the effect of accounting for both the macro and the micro components of the texture, rather than just the macro-texture, in the prediction of skid resistance."

Friction and texture data was collected from 28 different asphalt pavements in service in Texas, which presented different aggregate gradation. The pavements analyzed were located near Austin, Yoakum, and San Antonio. All test sections consisted of dense graded HMA pavements. Its selection intended to "obtain a final dataset that covers a wide range of friction coefficient 130 values and includes different cases for each possible combination of fine and coarse macro-131 texture and smooth and rough micro-texture" (Serigos et al., 2014).

Thus, measurements of texture and friction before and after applying texturing treatment were analyzed. The friction was characterized under wet conditions and in the direction of traffic using the British Pendulum Tester (ASTM E 303). The British Pendulum Number (BPN) was computed as the mean value of the individual BPN of five consecutive swings to eliminate any error that could be produced by the operator and wind conditions. The macro- and micro-texture were characterized by the CTM (ASTM E 2157) and LTS respectively. The MPD values were calculated using the data collected using each device. Texture data were always collected prior to friction in order to ensure dry condition during the scanning of the surfaces.

To characterize the pavement surface micro-texture, the data collected with the LTS was analyzed in the spectral/frequency domain and in the spatial domain. In the first case, the Discrete Fourier Transform was applied to separate macro- and micro-texture by isolating the different wavelength ranges. Using the power spectral density (PSD), the micro-texture was characterized

using the slope and the y-intercept of a linearized PSD (Figure 4.12). It was observed that the greater the intercept, the greater the surface friction, while the slope did not significantly affect it.

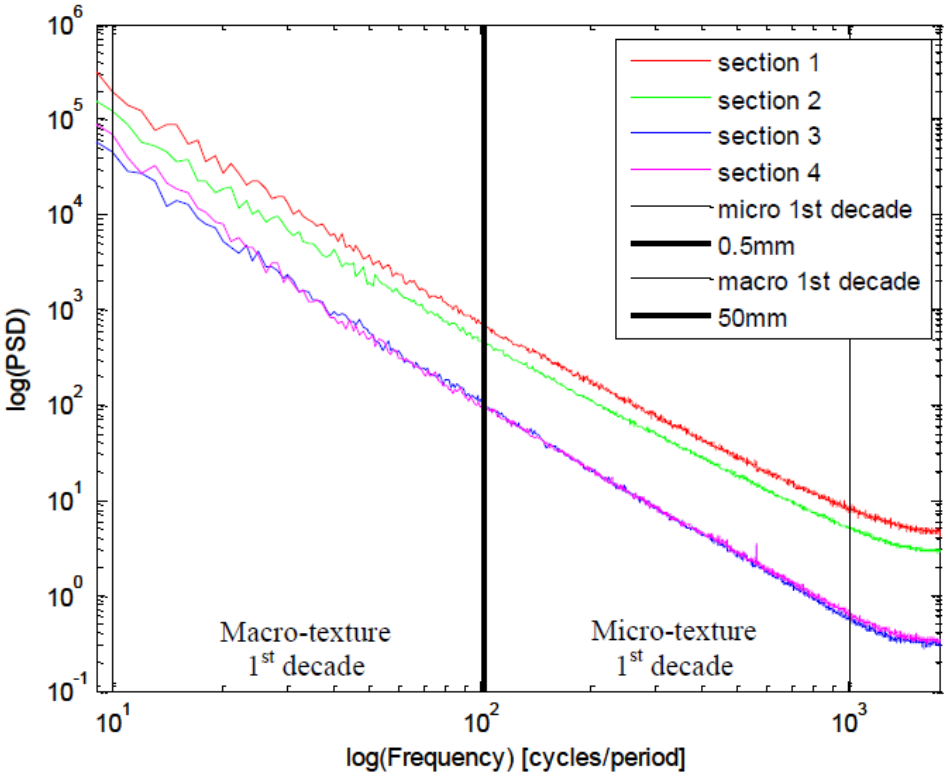

Figure 4.12: PSDs of four scanned surfaces.

In addition, the first decade of micro-texture (wavelengths between 0.05 mm to 0.50 mm) was analyzed in the spatial domain using parameters currently used to estimate the macro-texture (MPD and RMS), as well as parameters used in surface metrology (slope variance). Different baselines were analyzed as there is no current standard for micro-texture: 1 mm, 5 mm, 10 mm, and 20 mm (the LTS allowed to collect 70 points per mm). Profile standards of 100 mm in length are the standard for macro-texture.

The study suggested that baseline shorter than 10 mm resulted in a better prediction of the pavement surface friction. Among the parameters analyzed, the slope parameters were found to be better predictors of the surface friction than the amplitude parameters (MPD and RMS). However, among these parameters the MPD was better able to explain the friction.

Figure 4.13 shows the coordinates of a scanned line (in red) along with the filtered macro-texture (in green) and micro-texture profiles (in blue). The graph at the top (a) shows the coordinates for the entire 50.8 mm whereas the graph at the bottom (b) shows a close-up of the scanned line between the longitudinal coordinates of 35 mm and 40 mm to allow visualization of the surface in detail.

The profiles were normalized with respect to the average height, allowing consideration of only the active area of the pavement surface that will be in contact with the tires (elevations above the median height), which improved the friction prediction. The prediction of the friction using micro-texture spatial parameters calculated in the active area was as good as the one using the spectral parameters.

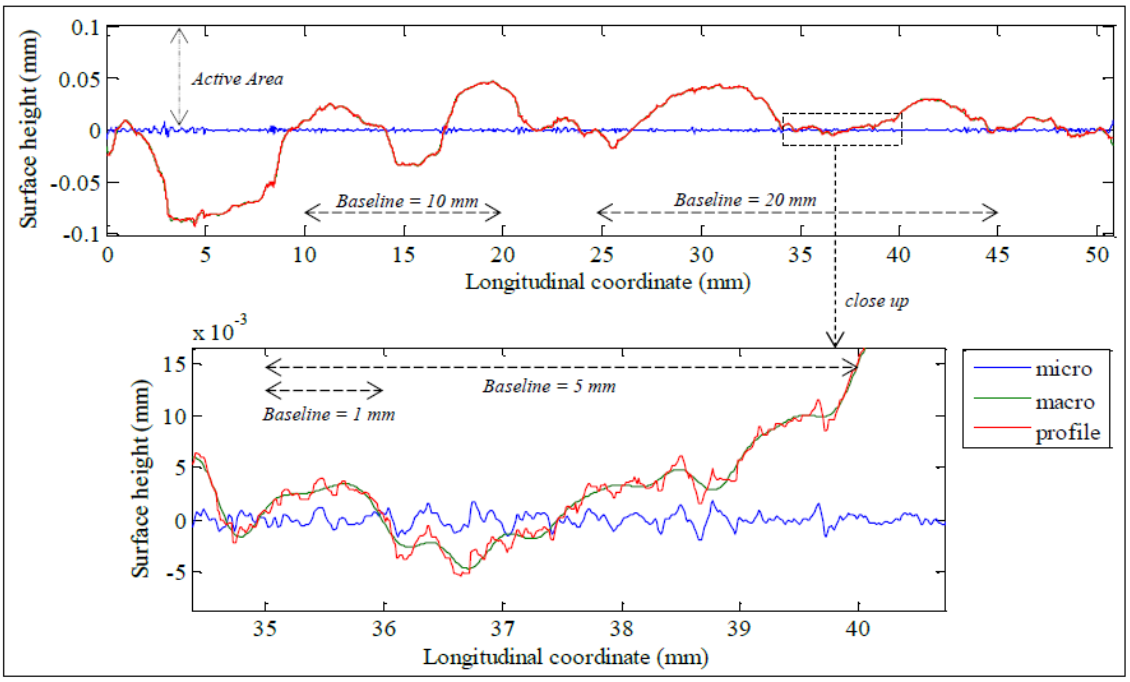

Figure 4.13: (a) Line scan of pavement surface with filtered micro and macro-texture components (above) and (b) close up of line scan profile (below) (Serigos et al., 2014).

As part of the study, it was concluded that "accounting for both the macro- and the micro-texture components of the surface will significantly enhance the prediction of BPN of flexible pavements as oppose to accounting solely for the macro-texture component. Such improvement will allow transportation agencies to better manage skid resistance and therefore to improve road safety" (Serigos et al., 2014).

4.5.5 Studies by the Institute of Highway Engineering

The study performed by the RWTH Aachen University (Ueckermann et al., 2014) analyzed different contactless skid resistance measurement in order to predict pavement friction from texture measurements using a tire-rubber friction model.

Two skid resistance measuring devices were chosen to prove the theoretical approach: the Wehner/Schulze (W/S) machine (Figure 4.14), which corresponds to a blocked-wheel braking test, and the ViaFriction device of Via Tech AS (Figure 4.15), which measures the skid resistance under controlled longitudinal slip and corresponds to ABS braking conditions (Ueckermann et al., 2014). Both devices measured skid resistance under wet conditions and at a speed of 37 mph (60 kph).

Figure 4.14: Wehner/Schulze device (a) overall view and (b) skid resistance measuring unit (Ueckermann et al., 2014).

Figure 4.15: Via Friction device (a) overall view and (b) ViaFriction measuring unit (Ueckermann et al., 2014).

For comparison with the W/S device, 33 different surfaces covering a wide range of friction coefficients (low and high roughness) were tested. Thirteen of these samples were washed concrete slabs made in the laboratory exhibiting different maximum aggregate sizes (8 and 11 mm) and different polishing treatments. The polishing was performed by the ARTe (Aechen Rafeling Tester). On the other hand, the rest of the samples were asphalt concrete (AC) cores obtained from actual road surfaces and parking lots comprising the same maximum aggregate sizes of the concrete slabs. Among those, only one of the samples was a stone matrix asphalt (SMA). For comparison with the ViaFriction device, only five different surfaces were tested: three SMA and two AC pavements These surfaces were very homogenous regarding their skid resistance.

Similar to the results found in Serigos et al., 2014, the linearized PSD was used to describe the wavelength or frequency dependency of the texture. In addition, a real contact area was considered, as the contact between tire and pavement surface only occurs on the top surface asperities. The study suggested that there is a close relationship between measured and predicted friction coefficients. Wavelengths between 1 mm and 60 micrometers were found to be crucial to explain the coefficient of friction from texture measurement. Due to both the temperature and the influence of the water, the friction that can be generated by the W/S device was found to be significantly lower than that of the ViaFriction device.

References

Ames Engineering Laser Texture Scanner. User Manual. Software version 9.0." Iowa: Ames Engineering, 2010.

AASHTO T 304. "Uncompacted void content method A." Washington, D.C.: American Association of State Highway and Transportation Officials, 2011.

ASTM D 4791. "Standard test for flat particles, elongated particles, or flat and elongated particles in coarse aggregates." Philadelphia, Pennsylvania: American Society for Testing and Materials (ASTM), 2010.

ASTM D 5821. "Standard Test Method for determining the percentage of particles in coarse aggregate." Philadelphia, Pennsylvania: American Society for Testing and Materials (ASTM), 2013.

ASTM D6928 "Standard Test Method for Resistance of Coarse Aggregate to Degradation by Abrasion in the Micro-Deval Apparatus." Philadelphia, Pennsylvania: American Society for Testing and Materials (ASTM), 2010.

ASTM E867 "Standard Terminology Relating to Vehicle-Pavement Systems." Philadelphia, Pennsylvania: American Society for Testing and Materials (ASTM), 2012.

ASTM E965 "Standard Test Method for Measuring Pavement Macrotexture Depth Using a Volumetric Technique." Philadelphia, Pennsylvania: American Society for Testing and Materials (ASTM), 2006.

ASTM E1845 "Standard Practice for Calculating Pavement Macrotexture Mean Profile Depth." Philadelphia, Pennsylvania: American Society for Testing and Materials (ASTM), 2009.

ASTM E2157 "Standard Test Method for Measuring Pavement Macrotexture Properties Using the Circular Track Meter." Philadelphia, Pennsylvania: American Society for Testing and Materials (ASTM), 2009.

Bathina. "Quality Analysis of the Aggregate Imaging System Measurements (AIMS)." Texas: Texas A&M University, 2005.

Chen, D. H., D. F. Lin and H. L. Luo. Effectiveness of Preventative Maintenance Treatments Using Fourteen SPS-3 Sites in Texas." *Journal of Performance of Constructed Facilities*, 17(3). 2003. pp. 136–143.

Elkins, G. E., P. Schmalzer, T. Thompson, and A. Simpson. *Long-Term Pavement Performance Information Management System, Pavement Performance Database User Guide*. Report No. FHWA-RD-03-088. Federal Highway Administration, Office of Infrastructure Research and Development, Washington, D.C., 2003.

Eltahan, A., J. Daleiden, and A. Simpson. Effectiveness of Maintenance Treatments of Flexible Pavements. In *Transportation Research Record: Journal of the Transportation Research Board*, *No. 1680*, Transportation Research Board of the National Academies, Washington, D.C., 1999, pp. 18–25.

Fletcher, Chandan, Masad, and Kumar. "Aggregate Imaging System (AIMS) for characterizing the shape of fine and coarse aggregates." Washington, D.C.: Transportation Research Board, 2003.

Flintsch, McGhee, de León Izeppi, and Najafi. "Surface Texture (Surface Roughness, Waviness, and Lay)." New York: ASME B46.1-2009, 2009

"Guidelines for Skid Resistant Pavement Design." Washington, D.C.: American Association of State Highway and Transportation Officials, Task Force for Pavement Design of the AASHTO Operating Subcommittee on Design, 1976.

Haider, S., and M. Dwaikat. Estimating Optimum Timing for Preventive Maintenance Treatment to Mitigate Pavement Roughness. In *Transportation Research Record: Journal of the Transportation Research Board*, *No. 2235*, Transportation Research Board of the National Academies, Washington, D.C., 2011, pp. 43–53.

Hall, K., C. Correa, and A. Simpson. Performance of Flexible Pavement Maintenance Treatments in the Long-Term Pavement Performance SPS-3 Experiment. In *Transportation Research Record: Journal of the Transportation Research Board*, *No. 1823*, Transportation Research Board of the National Academies, Washington, D.C., 2003, pp. 47–54.

Henry, J.J. "Comparison of Friction Performance of a Passenger Tire and the ASTM Standard Test Tires." Philadelphia, Pennsylvania: 1983.

Huang, Yang H. "Pavement Analysis and Design," 2nd Edition. New Jersey: Pearson/Prentice Hall, 2003.

Kleiber, C., and A. Zeileis. *Applied Econometrics with R*. New York: Springer-Verlag. 2008. http://CRAN.R-project.org/package=AER Accessed July 15, 2015.

Kulakowski, B.T., J.C. Wambold, C.E. Antle, C. Lin, and J.M. Mason. "Development of a Methodology to Identify and Correct Slippery Pavements" FHWA-PA90-002+88-06. State College, Pennsylvania: The Pennsylvania Transportation Institute, 1990.

LTPP InfoPave. *Standard Data Release*. http://www.infopave.com/Data/StandardDataRelease/ Accessed July 15, 2015.

Mahmoud, Gates, Masad, Erdoğan, and Garboczi. "Comprehensive evaluation of AIMS - Texture, Angularity & Dimension Measurements." Journal of Materials in Civil Engineering, ASCE, 2010.

Morian, D. A., G. Wang, D. Frith, and J. B. Reiter. Analysis of Completed Monitoring Data for SPS-3 Experiment. *Transportation Research Board 90th Annual Meeting*. Transportation Research Board of the National Academies, Washington, D.C., 2011.

Morian, D. A., S. D. Gibson, and J. A. Epps. *Maintaining Flexible Pavements – The Long-Term Pavement Performance Experiment SPS-3 5-Year Data Analysis*. Report No. FHWA-RD-97-102. Federal Highway Administration, Office of Infrastructure Research and Development, Washington, D.C., 1998.

Masad, Luce, and Mahmoud "Implementation of AIMS in Measuring Aggregate Resistance to Polishing, Abrasion and Breakage" Texas: Texas Transportation Institute, 2006.

Masad, Luce, Mahmoud, and Chowdhury. "Relationship of Aggregate Texture to Asphalt Pavement Skid Resistance Using Image Analysis of Aggregate Shape." http://onlinepubs.trb.org/onlinepubs/archive/studies/idea/finalreports/highway/nchrp114final_report.pdf. Washington, D.C.: Transportation Research Board, 2007.

Masad, Rezaei, and Chowdhury. "Field Evaluation of Asphalt Mixtures Skid Resistance and its Relationship to Aggregate Characteristics." http://d2dtl5nnlpfr0r.cloudfront.net/tti.tamu.edu/documents/0-5627-3.pdf .Texas: Texas Transportation Institute, 2010.

Masad, Rezaei, Chowdhury, and Harris. "Predicting Asphalt Mixture Skid Resistance Based On Aggregate Characteristics." Texas: Texas Transportation Institute, 2009.

Masad, "Aggregate Imaging System (AIMS) - Basics and Applications." Texas: Texas Transportation Institute, 2005.

McGhee, and Flintsch. "High-Speed Texture Measurement of Pavements." http://www.virginiadot.org/vtrc/main/online_reports/pdf/03-r9.pdf. Virginia: Virginia Transportation Research Council, 2003.

Moore, Desmond. Ph.D. Thesis "The sinkage of flat plates on smooth and rough surfaces." Pennsylvania: Pennsylvania State University, 1963.

NCHRP Report 634 "Texturing of Concrete Pavements." http://onlinepubs.trb.org/onlinepubs/nchrp/nchrp_rpt_634.pdf . Washington, D.C.: Transportation Research Board, 2009.

NCHRP Synthesis 291 "Evaluation of Pavement Friction Characteristics." http://onlinepubs.trb.org/onlinepubs/nchrp/nchrp_syn_291.pdf. Washington, D.C.: Transportation Research Board, 2000.

NCHRP Web-Only Document 108: "Guide for Pavement Friction." http://onlinepubs.trb.org/onlinepubs/nchrp/nchrp_w108.pdf . Washington, D.C.: Transportation Research Board, 2009.

Noyce, Bahia, Yambó and Kim. "Incorporating Road Safety Into Pavement Management: Maximizing Asphalt Pavement Surface Friction For Road Safety Improvements." http://www.wistrans.org/mrutc/files/Lit-rev-and-info.pdf. Midwest Regional University Transportation Center, 2009.

"Pavement Friction Management." http://www.fhwa.dot.gov/pavement/t504036.cfm. Washington, D.C.: Federal Highway Administration, 2005. http://www.fhwa.dot.gov/pavement/t504038.cfm. Washington, D.C.: Federal Highway Administration, 2010.

R Core Team. *R: A Language and Environment for Statistical Computing*. R Foundation for Statistical Computing, Vienna, Austria. 2014.

Rasmussen, Sohaney, Wiegan, and Harrington. Tech Brief "Measuring and Analyzing Pavement Texture." http://www.cptechcenter.org/technical-library/documents/sc/pavement_Texture_tech_brief_revised_2-25-2011_LQ.pdf . National Concrete Pavement Technology Center, Iowa State University, 2011.

"Report of the Committee on Surface Characteristics," Proceedings of the 18th World Road Congress. Brussels, Belgium: Permanent International Association of Road Congresses (PIARC), 1987.

Serigos, Smith, and Prozzi. TRB Paper 14-2278 "Incorporating Surface Micro-Texture in the Prediction of 3 Skid Resistance of Flexible Pavements." Washington, D.C.: Transportation Research Board.

Shirazi, H., R. L. Carvalho, M. Ayres Jr, and O. I. Selezneva. Statistical Analysis of LTPP SPS-3 Experiment on Preventive Maintenance of Flexible Pavements. *First International Conference on Pavement Preservation*. Newport Beach, CA. 2010.

"Superpave Asphalt Mixture Design" Workshop Washington, D.C.: Federal Highway Administration, 2002.

"The Little Book of Tire Pavement Friction" version 1.0. https://secure.hosting.vt.edu/www.apps.vtti.vt.edu/1-pagers/CSTI_Flintsch/The%20Little%20Book%20of%20Tire%20Pavement%20Friction.pdf Pavement Surface Properties Consortium, 2012.

Ueckermann and Wang. "Towards Contactless Skid Resistance Measurements." Aachen: RWTH Aachen University, Institute of Highway Engineering, 2014.

Wooldridge, J. M. *Econometric analysis of cross section and panel data*. MIT press, 2010.